DOT HS-806 960
DOT TSC NHTSA 85 4

Crash Padding R search
Volume I: Material Mechanical Properties

Oscar Orringer
Kevin T Knadle
John F Mandell

Transportation Systems Center
Cambridge MA 02142

July 1986
Final Report

US Department of Transportation
National Highway Traffic Safety Administration

Office of Research and Development
Office of Crashworthiness Research
Washington DC 20590

T chnical Rep rt Documentati n Page

1. Report No	2 Government Accession No	3. Recipient's Catalog No.
DOT-HS-806-960		

4. Title and Subtitle	5 Report Date
CRASH PADDING RESEARCH Volume I: Material Mechanical Properties	July 1986
	6 Performing Organization Code DTS-44
7 Author(s) Oscar Orringer, Kevin T. Knadle,* John F. Mandell*	8 Performing Organization Report No DOT-TSC-NHTSA-85-4
9 Performing Organization Name and Address U.S. Department of Transportation Research and Special Programs Administration Transportation Systems Center Cambridge, MA 02142	10 Work Unit No (TRAIS) HS676/S6508
	11 Contract or Grant No
	13 Type of Report and Period Covered Final Report April 1982-June 1984
12 Sponsoring Agency Name and Address U.S. Department of Transportation National Highway Traffic Safety Administration Office of Research and Development Washington, DC 20590	14 Sponsoring Agency Code NRD-10

15 Supplementary Notes *Department of Materials Science and Engineering
Massachusetts Institute of Technology
Cambridge, MA 02139

16 Abstract

The dynamic mechanical properties of Uniroyal Ensolite AAC, a viscoelast. closed-cell foam rubber, are investigated by means of materials tests. Sufficient test data is presented to form a basis for one-dimensional (uniform compression) empirical constitutive equation models. Results of some additional tests are presented to assess the potential usefulness of a one-dimensional constitutive equation for predicting response in typical occupant-to-vehicle impact situations.

17. Key Words	18. Distribution Statement
Crash Padding, Mechanical Properties, Materials Testing, Viscoelastic Materials, Rubber, Foam Rubber	Document is available to the public through the National Technical Information Service, Springfield, VA 22161

19. Security Classif. (of this report)	20. Security Classif. (of this page)	21. No. of Pages	22. Price
Unclassified	Unclassified	64	

Form DOT F 1700.7 (8-72) Reproduction of completed page authorized

PREFACE

The analytical work described herein was conducted at the DOT Transportation Systems Center, Cambridge, Massachusetts. The experimental work was conducted at the Massachusetts Institute of Technology, Cambridge, Massachusetts. The work was sponsored by the National Highway Traffic Safety Administration under Project Plan Agreement HS-476. This series of reports is specifically concerned with evaluating the impact response characteristics of foam-type crash padding materials. This report is the first of three volumes in the series. This report covers the results of laboratory tests to determine the basic dynamic mechanical properties of a typical foam rubber. Volume II will cover the derivation of foam-rubber constitutive equation models and the procedures used to fit the model parameters to the laboratory test results. Volume III will cover application and validation of the best model for impact response prediction.

METRIC CONVERSION FACTORS

Approximate Conversions to Metric Measures

Symbol	When You Know	Multiply by	To Find	Symbol
LENGTH				
in	inches	*2.5	centimeters	cm
ft	feet	30	centimeters	cm
yd	yards	0.9	meters	m
mi	miles	1.6	kilometers	km
AREA				
in^2	square inches	6.5	square centimeters	cm^2
ft^2	square feet	0.09	square meters	m^2
yd^2	square yards	0.8	square meters	m^2
mi^2	square miles	2.6	square kilometers	km^2
	acres	0.4	hectares	ha
MASS (weight)				
oz	ounces	28	grams	g
lb	pounds	0.45	kilograms	kg
	short tons (2000 lb)	0.9	tonnes	t
VOLUME				
tsp	teaspoons	5	milliliters	ml
Tbsp	tablespoons	15	milliliters	ml
fl oz	fluid ounces	30	milliliters	ml
c	cups	0.24	liters	l
pt	pints	0.47	liters	l
qt	quarts	0.95	liters	l
gal	gallons	3.8	liters	l
ft^3	cubic feet	0.03	cubic meters	m^3
yd^3	cubic yards	0.76	cubic meters	m^3
TEMPERATURE (exact)				
°F	Fahrenheit temperature	5/9 (after subtracting 32)	Celsius temperature	°C

*1 in. = 2.54 cm (exactly). For other exact conversions and more detail tables see NBS Misc. Publ. 286, Units of Weight and Measures. Price $2.25 SD Catalog No. C13.10:286.

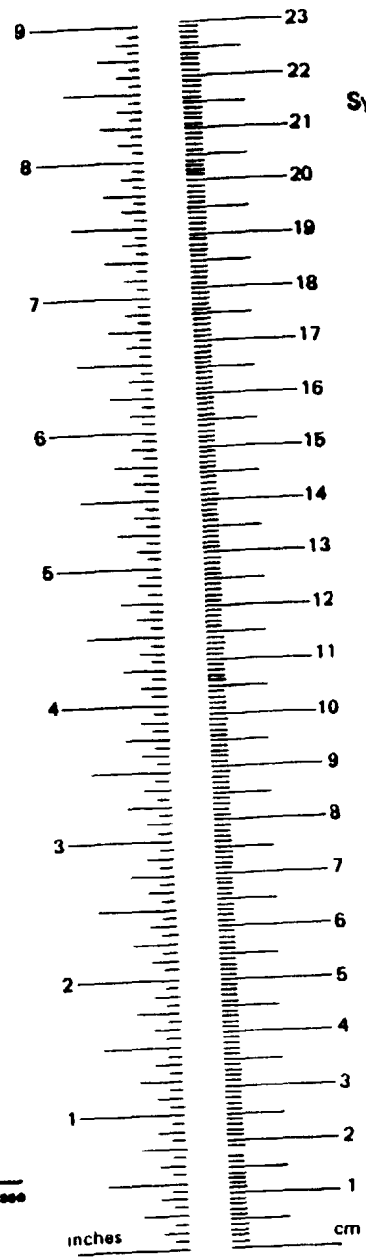

Approximate Conversions from Metric Measures

Symbol	When You Know	Multiply by	To Find	Symbol
LENGTH				
mm	millimeters	0.04	inches	in
cm	centimeters	0.4	inches	in
m	meters	3.3	feet	ft
m	meters	1.1	yards	yd
km	kilometers	0.6	miles	mi
AREA				
cm^2	square centimeters	0.16	square inches	in^2
m^2	square meters	1.2	square yards	yd^2
km^2	square kilometers	0.4	square miles	mi^2
ha	hectares (10,000 m^2)	2.5	acres	
MASS (weight)				
g	grams	0.035	ounces	oz
kg	kilograms	2.2	pounds	lb
t	tonnes (1000 kg)	1.1	short tons	
VOLUME				
ml	milliliters	0.03	fluid ounces	fl oz
l	liters	2.1	pints	pt
l	liters	1.06	quarts	qt
l	liters	0.26	gallons	gal
m^3	cubic meters	36	cubic feet	ft^3
m^3	cubic meters	1.3	cubic yards	yd^3
TEMPERATURE (exact)				
°C	Celsius temperature	9/5 (then add 32)	Fahrenheit temperature	°F

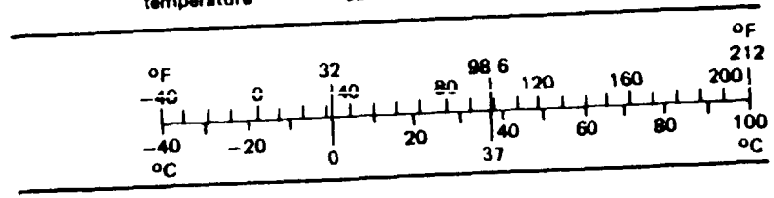

TABLE OF CONTENTS

LIST OF FIGURES

LIST OF TABLES

SUMMARY

Selection of materials for energy-absorbent performance is an important consideration for automobile interior padding, which must provide the greatest occupant protection for the least padding thickness possible. Rational selection requires an understanding of which material properties, as measured in standard laboratory tests, correlate well with impact performance in crash situations. Such understanding can be gained by characterizing a material in the laboratory, constructing a performance model from the laboratory test results, applying the model to predict the response of the material to impact conditions, and then verifying the prediction by test. This report summarizes the results of the first link in the chain of understanding.

A program of laboratory experiments was undertaken to characterize the dynamic mechanical properties of Uniroyal Ensolite AAC foam rubber. This material is a typical padding product, and has been used by the National Highway Traffic Safety Administration in other experimental investigations of injury mitigation concepts for automobile occupants.

The present test program was designed to evaluate a hypothesis that standard laboratory test methods could be used to measure the properties which correlate with impact performance. The test program thus emphasized the material properties associated with uniform compression of small samples. Additional tests were performed, however, to investigate the material under more complex loading conditions in order to evaluate the potential usefulness of the uniform-compression model.

The results of this research program are as follows:

- Sufficient standard data have been gathered to provide the basics required for modelling the dynamic behavior of Ensolite AAC foam rubber in uniform comparison.
- It appears that useful predictions of impact response should be possible, based on a uniform-compression material model.
- Sufficient nonstandard test data have been gathered to provide for understanding of prediction errors, i.e. to identify any significant material properties not included in the uniform-compression model.
- An experimental protocol applicable to the characterization of other crash padding materials has been established.

1. INTRODUCTION

Automobile interior crash padding is used to protect vehicle occupants against serious injury during collisions, when parts of the occupant's body may strike parts of the vehicle's interior structure. The padding should ideally provide high energy absorption at low force levels, but practically its performance is limited for general ride comfort. Material selection for energy-absorbent performance thus becomes an important consideration.

Since an occupant-to-vehicle impact typically consumes only 20 to 50 milliseconds (ms), the dynamic properties of the material at short times (or equivalently, high strain rates) determine its energy-absorption characteristics. Candidate padding materials are typically viscoelastic, i.e. they relax under load, their moduli are time-dependent, and their dynamic properties are strongly dependent on strain rate.

The behavior of real materials is also considerably more complex than the descriptions afforded by simplified hypothesis such as linear viscoelastic models. Hence, standard rheological test methods must be applied to experimentally characterize the behavior of a real material, but the tests must be made at or near strain rates corresponding to typical occupant-to-vehicle impacts. Only after data has been obtained from such tests is it possible to construct a good empirical model of the material behavior.

The present work started with a laboratory experiment program on Uniroyal Ensolite AAC, a recoverable closed-cell foam rubber material which has been used in previous NHTSA investigations of injury-reduction concepts for automobile passenger compartments. This report summarizes the experimental methods which were used to characterize Ensolite foam and the results of the tests.

Experimental data is to be used to define several parameters of an empirical equation representing the time-dependent relaxation, loading, and unloading behavior of the foam. Therefore, to effectively model the impact-rate collision of unrestrained occupants with padded structures, test data should cover peak strains of at least 0.8, strain rate as high as 2000 per second, and relaxation times down to 0.1 ms. The experimental objective is to characterize the compressive response of the material. Specifically, the type of data sought include stress relaxation curves for at least three different strains, and full stress-strain loading and unloading curves at various strain rates from which can be derived stress versus strain rate, percent residual strain versus strain rate, and asymptotic (fully relaxed) stress-strain curves.

Initial attempts to directly measure the material performance could not reach impact rates without introducing spurious test fixture vibrations into the data. Therefore, tests were ultimately conducted at somewhat lower strain rates but also at lower temperatures, and the time-temperature superposition principle was used to extrapolate the data. Unless otherwise noted, the test specimens were cut 1.38 inches in diameter from 0.14 inch thick Ensolite sheets. The tests were performed on both electromechanical (EM) and servohydraulic (SH) machines.

Sections 2 and 3 describe the procedures used and the results obtained in two types of standard materials tests: the stress-relaxation test and the stress-strain test. These results provide the data necessary for fitting a one-dimensional (uniform compression) constitutive equation model to the material. The extent to which such a model is useful for predicting behavior when the material is subjected to nonuniform impact conditions depends upon other properties. Section 4 describes some additional experiments which were performed to address this question.

2. STRESS-RELAXATION EXPERIMENTS

If a compressive strain is suddenly imposed on a viscoelastic test specimen and then held constant, the stress developed in the specimen will relax with time. For example, the stress σ (t) in an ideally linear viscoelastic material responding to a strain ε applied suddenly at t = 0 is given by [1] :

$$\sigma(t) = E_\infty \varepsilon + (E_0 - E_\infty)\varepsilon e^{-t/\tau} \tag{1}$$

The parameters E_0 and E_∞ are, respectively, an instantaneous elastic modulus and a fully relaxed elastic modulus, while the parameter τ is a characteristic decay time.

Equation 1 is a solution of the first-order differential equation:

$$\dot{\sigma} + \sigma/\tau = E_0 \dot{\varepsilon} + E_\infty \varepsilon/\tau \tag{2}$$

where a dot over a quantity indicates a time derivative. Equation 2 describes a state or constitutive relationship between stress, strain, and the time rates of change of stress and strain. Equation 1 is the solution of Equation 2 for the special conditions: ε =constant, $\dot{\varepsilon} = 0$ for $t \geq 0$; and $\sigma = E_0 \varepsilon$ at t = 0.

The foregoing equations might be used to model real materials, but the parameter values which fit long-time data do not necessarily fit short-time data. Hence, it is desirable to perform stress-relaxation experiments as close to the time range of interest as possible. Also, the experiment itself is complicated by the fact that real testing machines require a finite amount of time to apply the initial strain.

2.1 DIRECT MEASUREMENT AT IMPACT SPEEDS

Measuring stress relaxation data at impact rates involves reading force* values from a load cell immediately after loading a specimen, in less than one ms, to a given

*Force is converted to engineering stress by using the cross-section area of the uniformly loaded specimen as a scale factor. Also, engineering strain is defined as total compression displacement scaled by the undeformed thickness of the specimen.

strain. The specimen was in the form of a short cylinder mounted directly on the load cell to minimize dynamic effects in the apparatus. In general, it was not difficult to attain the desired range of loading rate with rubber cords or hand-swung hammers. The major problem was dynamic ringing of the apparatus and specimen during the load application and initial relaxation. To eliminate or reduce this ringing, which made short-time relaxation stress impossible to read, the following loading schemes were investigated, all using a high speed piezoelectric load cell and Nicolet digital oscilloscope.

a. Acceleration of a small loading disk with rubber cords followed by contact with a rigid stop which allowed a controlled strain to be imposed and held on the specimen.

b. Drop-weight apparatus with initial acceleration of the weight; weight either bounced on specimen or held from bouncing by ratchet device.

c. Forceful hand loading against a rigid stop to a fixed strain.

d. Dropping weight onto a wedge to fix maximum displacement without bounce.

e. Other hand and rubber cord schemes to investigate the sources of ringing in the system.

Figure 2-1 is a schematic example of the typical ringing that obscured the stress data. The first arrangement showed the greatest ringing effects due in part to noise transmission through the EM or SH machines which were used to load the rubber cords and on which the specimen was mounted. Other sources of ringing, such as pulsation of the rubber cords, were identified and greatly reduced or eliminated in later arrangements.

However, the most persistent problem was dynamic effects in the specimen itself. Whenever the specimen is rapidly compressed by a rigid member, and the movement of the member is abruptly terminated by contact with a rigid stop, the specimen continues to bounce and obscure the stress data for the order of 10 to 20 ms. An attempt to eliminate this problem using an electromagnetic device to stop and hold a drop weight just as its direction of movement reverses still did not reduce the ringing. The only clean load traces were obtained by allowing the loading weight or device to compress specimen and then rebound freely. While not useful for stress relaxation study since displacement is not held, this procedure did allow direct measurement of load-time data at impact rates and was thus useful for confirming stress-strain test results.

In summary, the requirements for direct measurement of stress-relaxation are that the strain be applied and any noise damped out within 0.1 to 1 ms. While methods of

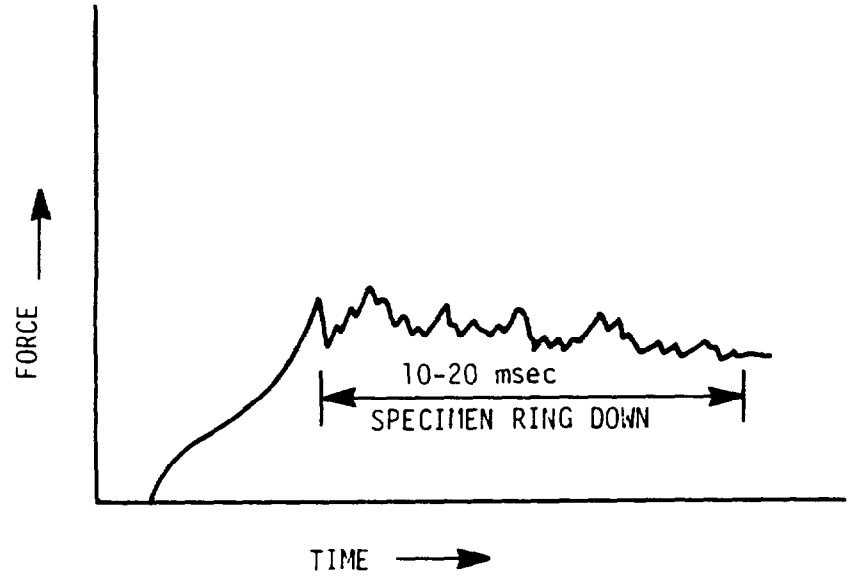

FIGURE 2-1. SCHEMATIC LOAD-TIME TRACE OF SHORT-TIME STRESS-RELAXATION EXPERIMENT

obtaining the desired velocity and instrumentation for recording data were readily developed, dynamic ringing of the apparatus and specimen made reading of the stress signal impossible through the first 10 ms of relaxation. Therefore, the investigation was shifted to longer times coupled with time-temperature superposition.

2.2 TIME-TEMPERATURE SUPERPOSITION

The dynamic properties of viscoelastic materials arise from molecular-level dissipation mechanisms. These mechanisms are controlled by molecular motions which are thermally driven and thus proportional to absolute temperature. Performing an experiment at a reduced temperature is, therefore, thermally equivalent to observing in an earlier time window or testing at a higher strain rate at a reference temperature. The time-temperature superposition principle applies these concepts by using a series of tes s at different temperatures to infer time- or rate-dependent behavior at the reference temperature [2, 3] .

The shifting of time scales is usually done graphically rather than by theoretical methods which apply mostly to linear amorphous polymers at low strains. In practice, the time-temperature shifts are empirically constructed by using overlapping sets of data to establish the continuity of trends and are confirmed where possible by comparison with data from direct measurements in the extended time domain [3] .

For foamed polymers such as Ensolite, time-temperature superposition, must be applied with particular caution because of the possible complications such as air-flow effects at certain rates, temperature effects on the pressure in closed cells, and crushing or buckling of cell walls. These effects may not be time-temperature shiftable even if the basic response of the material itself is shiftable.

2.3 EXPERIMENTAL PROCEDURE

Speciments 1.38 inches in diameter were die-cut from a 0.14 inch thick Ensolite sheet and placed between flat platens of the SH testing machine. Specimens were conditioned at the test temperature for at least 30 minutes. The strain was then applied to a predetermined level as quickly as possible and held constant at that value. Short-time displacements and forces were recorded on and read from a Nicolet oscilloscope. The oscilloscope results were also used to check actual displacement and to define a start-clock point. The complete relaxation force curve for the range 0 to 1000 seconds was recorded on a MINC 11/23 computer and a chart recorder.

The start-clock point was arbitrarily chosen at the point of maximum force upon reaching final displacement. Of course, relaxation had already begun before this point; the ideal stress relaxation test should begin with the strain imposed instantaneously, therefore relaxation data from finite displacement-rate tests should not be used for analysis until after a period of approximately three times the time required to reach the test strain. The SH machine delivered strain rates of approximately 6 to 8 in/sec; rates up to 140 in/sec were possible but did not allow immediate stopping and holding of the strain without dynamic effects. At 6 to 8 in/sec, maximum displacement occurred within 20 ms, and force data were read beginning at approximately 100 ms.

2.4 TEST RESULTS

The stress-relaxation test results at various strains, times, and temperatures are tabulated in Appendix A. Figure 2-2 illustrates the time-temperature shifting of individual curves at different temperatures into one master curve for room-temperature (25°C) behavior at 0.33 strain. Figure 2-3 presents the final 0.33, 0.50, and the 0.75 strain master curves with a different symbol representing data from each of the 25°C, 14°C, 1°C and -10°C temperature curves. Starting with the 25°C curve as a reference, master curves are constructed by sequentially shifting lower temperature curves to the left until they are judged to line up with the previously shifted higher temperature data. The shift factors used for each construction are plotted in Appendix B as a function of test temperature.

As indicated in Figure 2-2, the construction of the 0.33 strain master curve proceeded smoothly i.e., the curve at each temperature overlapped some and extended to the left of the preceding curve so that one smooth curve extending down through 0.01 ms resulted. The 0.50 strain data also shifted well except for some scatter in the 1°C and 14°C curves.

However, at 0.75 strain the individual temperature curves did not shift into one smooth curve. The smoothest possible shift was obtained by favoring the short-time ends of the individual curves. The master curve given in Figure 2-3 was constructed in this manner. If correct, this construction suggests that low test temperatures cause the stress at 0.75 strain to relax more quickly than at other combinations of temperature and strains. These specimens also show some long-lasting deformation after the strain is removed. These results suggest some other mechanism of deformation, such as cell wall crushing, which is not shiftable from low temperatures to short time or high strain rate.

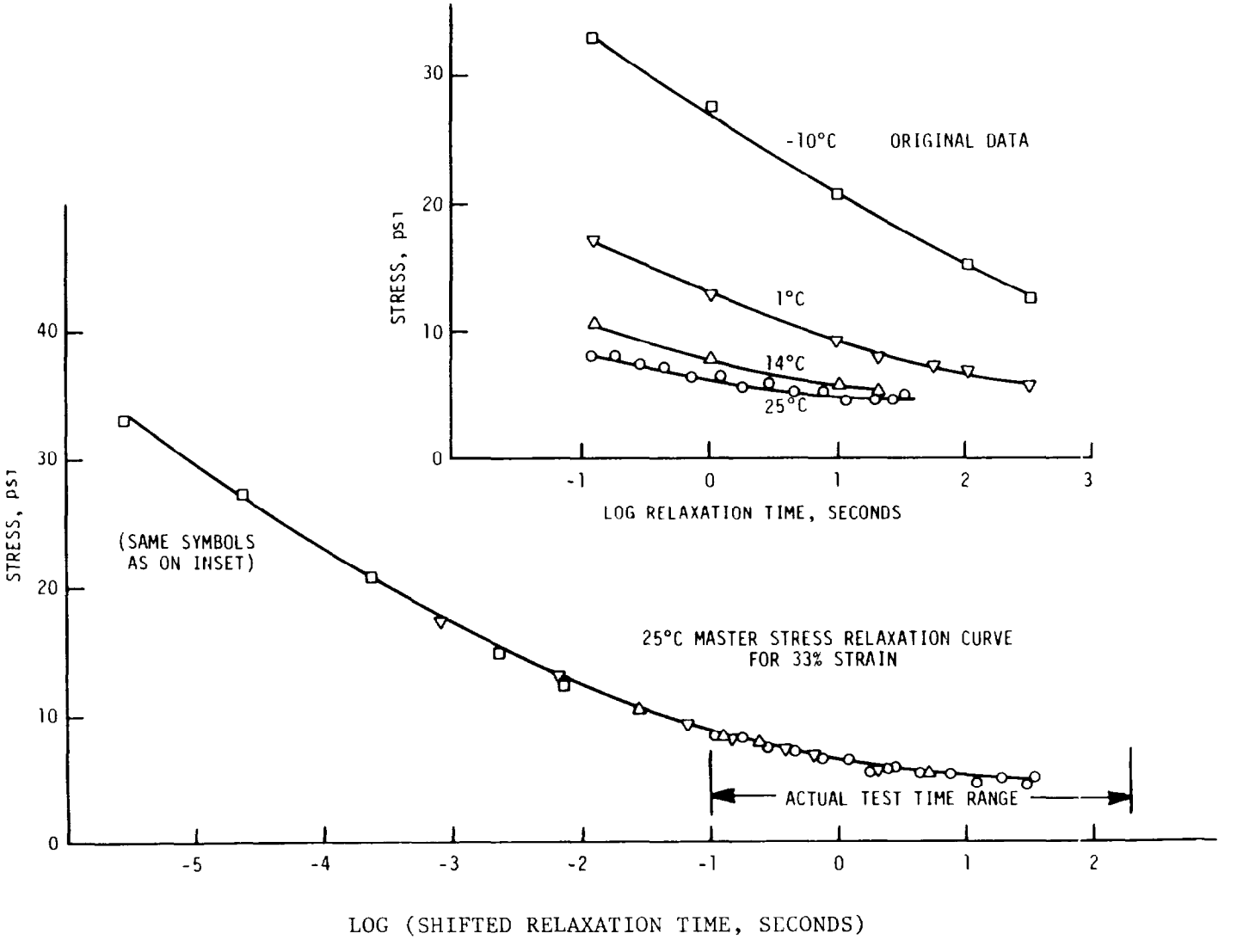

FIGURE 2-2. CONSTRUCTION OF MASTER STRESS RELAXATION CURVE FROM ORIGINAL DATA
(33% strain, 25° C compression, thin Ensolite AAC foam)

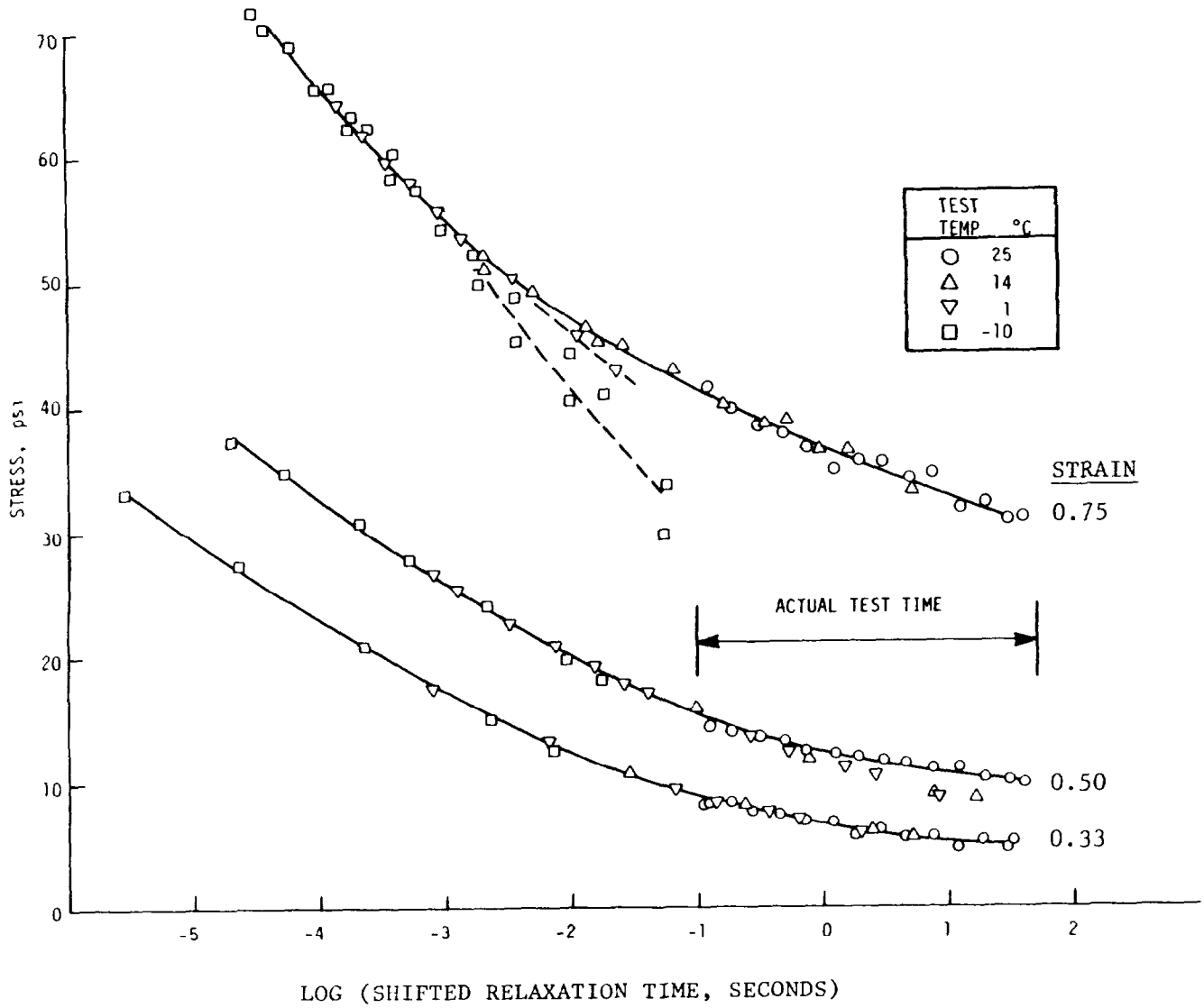

FIGURE 2-3. MASTER STRESS RELAXATION CURVES (25° C REFERENCE TEMPERATURE)

Figure 2-4 compares the master curves from Figure 2-3 with data representing the fastest 25°C stress relaxation tests which could be run without significant dynamic effects, although strain overshoot caused some difficulty in interpretation. The actual relaxation data at 0.33 strain compares well with the master curve. At 0.5 strain there is some deviation, but the general trend is similar. The 0.75 strain data are in good agreement at the shortest time, but at longer times, the data are scattered and also deviate downward much like the low-temperature data in Figure 2-3. In both Figures 2-3 and 2-4, deviation is significant only at times well beyond those of interest in impacts and the actual data agree well with master curve predictions at all three strains as impact rates are approached.

The complications cited may cause concern about the use of time-temperature superposition for Ensolite or for foams in general. However, the data is given for a very broad time scale, far beyond that necessary for the impact problem. While there is reason for caution, the stress-relaxation test results, when combined with the stress-strain test data in the next section, generally support the use of time-temperature shifting for prediction of short-time performance.

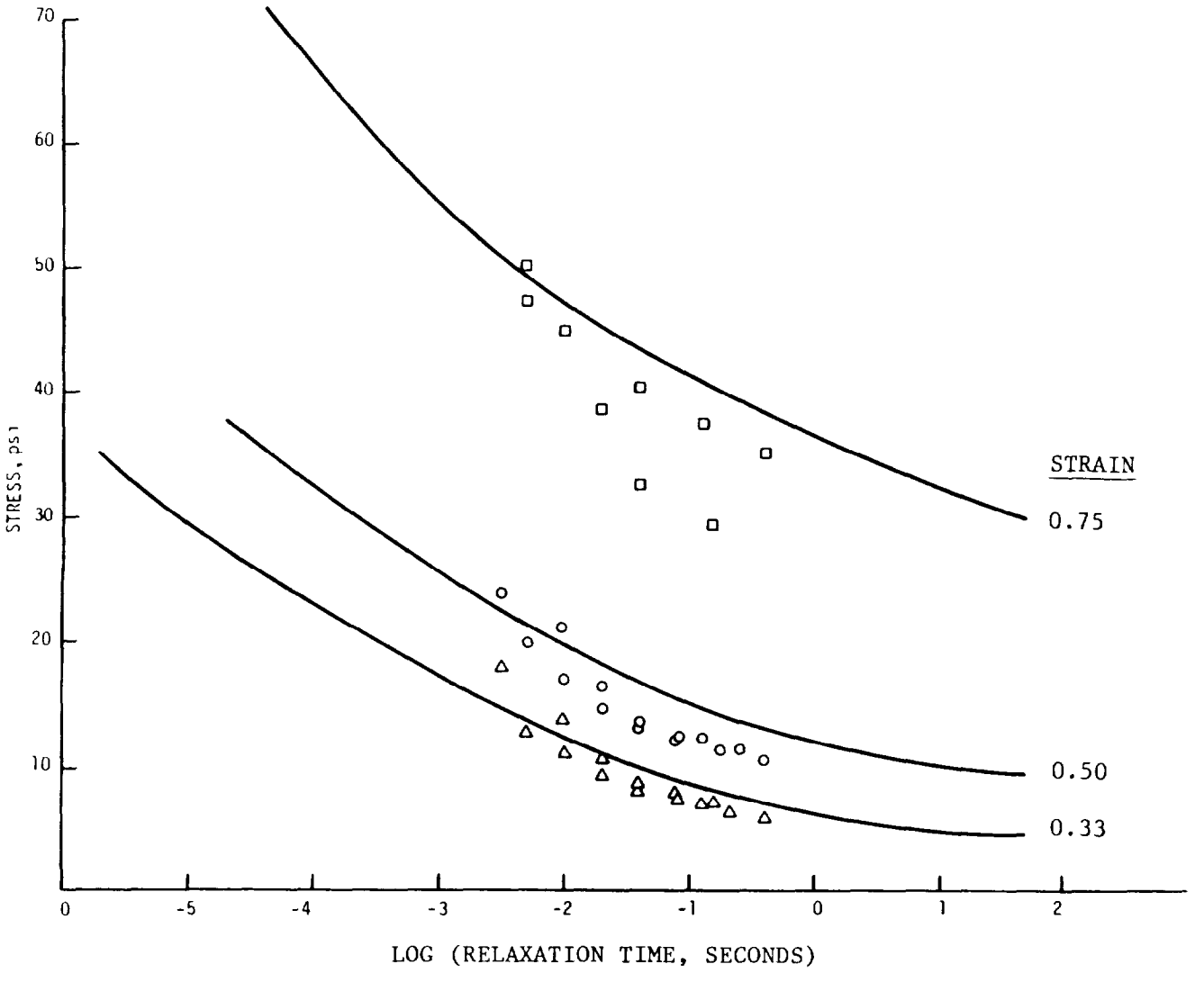

FIGURE 2-4. COMPARISON OF SHORT-TIME STRESS-RELAXATION TEST DATA WITH MASTER CURVES (25°C Reference Temperature)

3. STRESS-STRAIN EXPERIMENTS

In the stress-strain test, strain is applied at a constant rate until some predetermined maximum strain is reached. the testing machine is then rapidly reversed, and the applied strain is decreased at the same rate. Measurements of stress and strain can then be made for both the loading and unloading behavior.

For an ideally linear viscoelastic material (see Section 2.), the condition $\dot{\varepsilon}$ = constant for $t \geq 0$ can be applied to Equation 2 to represent the loading behavior. The corresponding solution of the constitutive equation is:

$$\sigma(t) = \left[E_\infty + (E_0 - E_\infty)\left(\frac{1-e^{-t/\tau}}{t/\tau}\right)\right]\varepsilon(t) \tag{3}$$

where (t) = $\geq$t. the quantity in brackets in Equation 3 can be recognized as a time-dependent modulus. Another way to visualize this response is to pose the question: "What stress is developed in the material at the time when a specific value of strain, ε, is reached?" This time is given by $t = \varepsilon/\dot{\varepsilon}$, and substitution of this relation in Equation 3 leads to:

$$\sigma(\varepsilon,\dot{\varepsilon}) = E_\infty \varepsilon + (E_0 - E_\infty)(1-e^{-\varepsilon/\dot{\varepsilon}\tau})\dot{\varepsilon}\tau \tag{4}$$

In a similar manner, one can solve Equation 2 for the unloading behavior by prescribing initial values of stress and strain together with the rate of strain decrease. In this case, the solution is such that a "residual" strain remains at the instant when the stress in the material has decreased to zero, i.e. the loading-unloading response is a hysteresis loop. The hysteresis loop is related to the stress-relaxation characteristic and to the material's ability to absorb energy in dynamic situations.

The general stress-strain response characteristics of a real material will follow the foregoing ideal model, but the details of the material's behavior will be more complex. Like the case of stress-relaxation, stress-strain tests are necessary to provide the data on which an empirical material model can be based.

There is also a subtle difference between the real materials and the ideally linear viscoelastic material. Examination of Equations 1 and 4 shows that all of the parameters required to define a constitutive equation for the ideal material can be derived from one type of test: either stress-relaxation or stress-strain. However, data from both types of test are required to define the equation of a real material.

3.1 EXPERIMENTAL PROCEDURE

Stress-strain curves were obtained using the same test apparatus as that described for stress relaxation tests. Specifically, the SH machine performed those tests with strain rates between 1.2 and 73 per second, while the EM machine performed the lower strain-rate tests (down to .0012 per second) including low temperature tests for time-temperature superposition. The strain-rate magnitude was kept constant during each test by using a triangle-shaped displacement-controlled loading and unloading function to a maximum strain between 0.75 and 0.85. No delay was allowed between the loading and unloading stages apart from unavoidable rounding of the triangular shape at the maximum point at the higher displacement rates.

Some stress-strain-time points were also obtained with an impact rig, which allowed specimens to be loaded by a hand-swung hammer to an adjustable maximum strain. A peizoelectric load cell directly below the specimen produced a force-time curve on the digital oscilloscope, from which the force and time at the point of peak strain could be read. The rate of applied strain was assumed to be constant and was calculated as strain/time at the peak point.

3.2 TEST RESULTS

The first series of tests measured low strain-rate EM loading-unloading curves at several cold temperatures for the purpose of constructing master curves, as done with the stress-relaxation data. Stacks of four thin foam specimens were subjected to the triangular displacement at strain rates on the order of 0.12 per second. Figure 3-1 illustrates the stress-strain curves obtained from these tests. The strong temperature-dependence of the hysteresis property evident in this plot implies an equivalent dependence on strain rate at fixed temperature.

In order to apply the time-temperature superposition principle to the construction of stress-strain master curves, it is more convenient to plot stress versus strain rate for several different values of strain, i.e. following the format suggested by Equation 4. The loading portions of the three highest temperature stress-strain curves in Figure 3-1 were thus cross-plotted to produce the data points shown in Figure 3-2. These data points correspond to strains of 0.33, 0.50, and 0.75, i.e. the same values used to plot stress-relaxation data, and they have already been time-temperature shifted. Also shown in Figure 3-2 are the master curves which were constructed from the data.

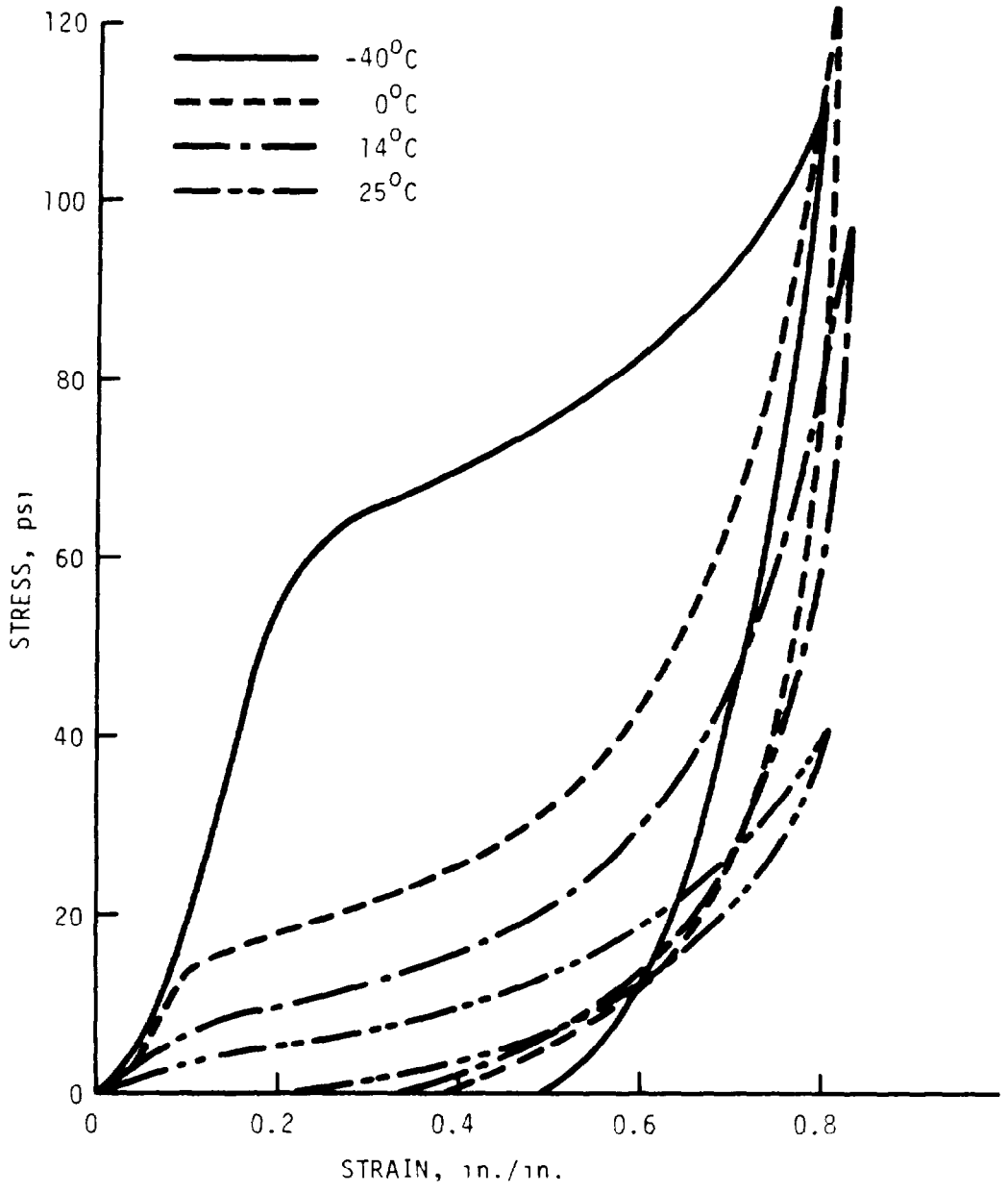

FIGURE 3-1. TYPICAL STRESS-STRAIN CURVES AT LOW STRAIN RATE

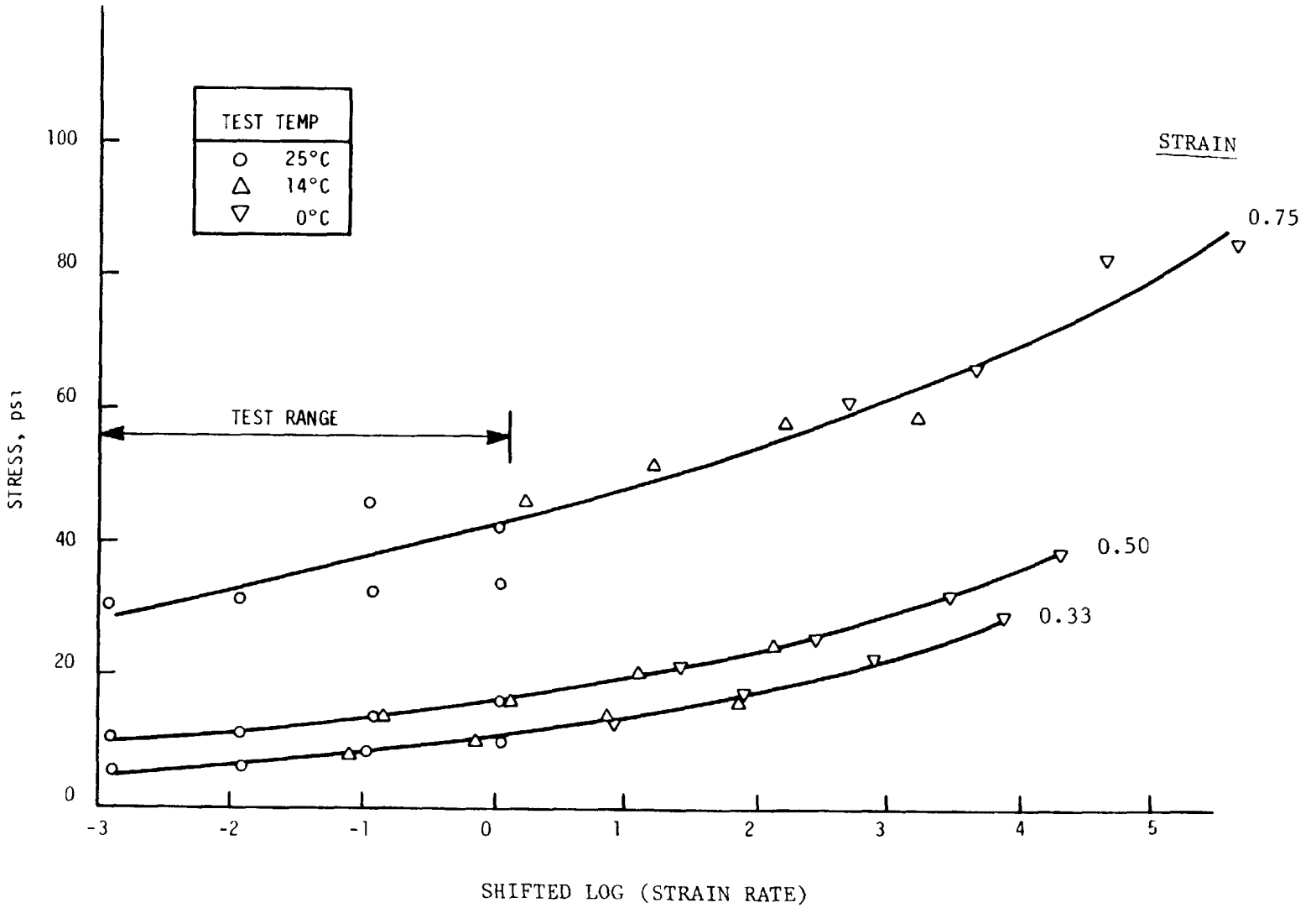

FIGURE 3-2. STRESS-STRAIN MASTER CURVES FROM LOW RATE TESTS (25°C Reference Temperature)

Just as stress-relaxation master curves must be confirmed by correlating their extrapolations with short-time measurements (see Section 2.4 and Figure 2-4), so also must stress-strain master curves be confirmed by comparison withs tests at high strain rates. Figure 3-3 compares the low-rate master curve predictions with higher-rate SH test results and impact-rig data. The latter data were primarily generated on single-layer specimens of the thin foam, with exceptions noted by the number of layers given in parenthesis next to some points. Single-thickness foam specimens were observed to give slightly higher stress values where SH data overlapped the original test speed range. (The constraint at the specimen/platen interface appears to stiffen the thinner specimens.) This is most evident at 0.75 strain. In general, the results in Figure 3-3 support the use of time-temperature shifting from slow tests into the impact speed range.

The energy absorbed by the foam, an important factor in collisions, is represented by the area between the loading and unloading curves. Figures 3-2 and 3-3 represent only the loading part of the stress-strain curve. The stress-strain curves in Figure 3-1 indicate a significant increase in hysteresis as the temperature decreases or the strain rate increases. Figure 3-4 plots the width of the hystresis loop at a stress of 20 psi and Figure 3-5 gives the residual strain at zero load. (The foam continues to recover after unloading, usually approaching its original thickness if left at room temperature.) The dashed portions of the 25°C lines are extrapolations based on the trend of 0°C data. At strain rates above 100 per second, the data from both figures appear to approach a width in the range 0.5 to 0.6 strain. Note that the hysteresis loop at 25°C changes width rapidly with rate in the strain-rate range of 1 to 1000 per second, which corresponds to a total test time of 1 second to 1 ms. This is the same range where the stress relaxation data deviate from superposition at 0.75 strain, and may represent the same underlying effect.

The stress-strain test results are tabluated in Appendix B. This appendix also contains a plot of the time-temperature shift factors which were used to construct both the stress-relaxation and stress-strain master curves.

3.3 COMPARISON OF RESULTS

The stress relaxation and stress-strain data should represent the same molecular relaxation processes in the polymer, and should, therefore, have similar trends with time. The lack of linear viscoelasticity, particularly at high strains, makes it impossible to relate the two sets of data in any simple quantitative fashion. For a given strain, however, the time required for decay to a given stress in a stress-relaxation test should

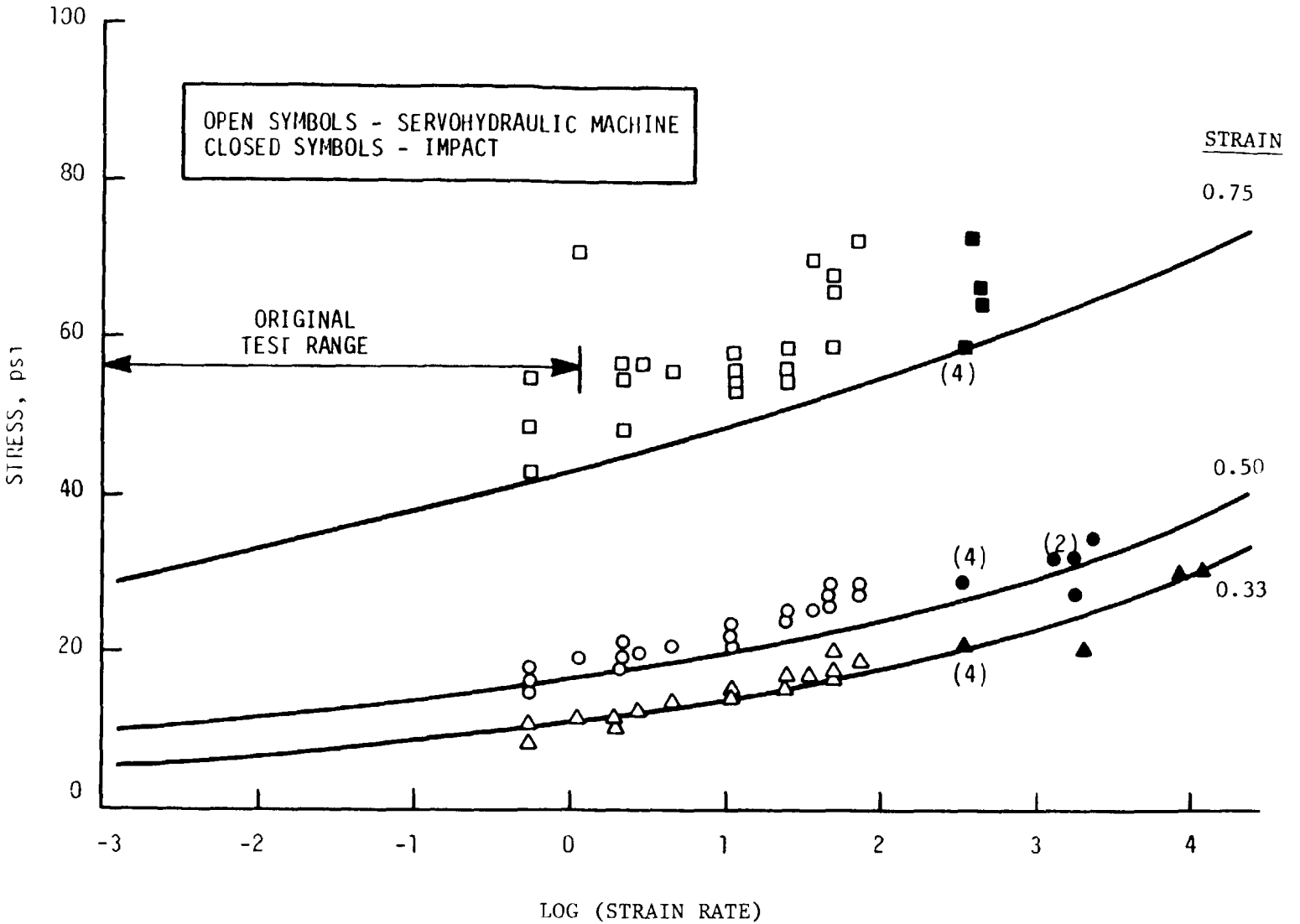

FIGURE 3-3. COMPARISON OF HIGH-RATE STRESS-STRAIN TEST DATA WITH MASTER CURVES

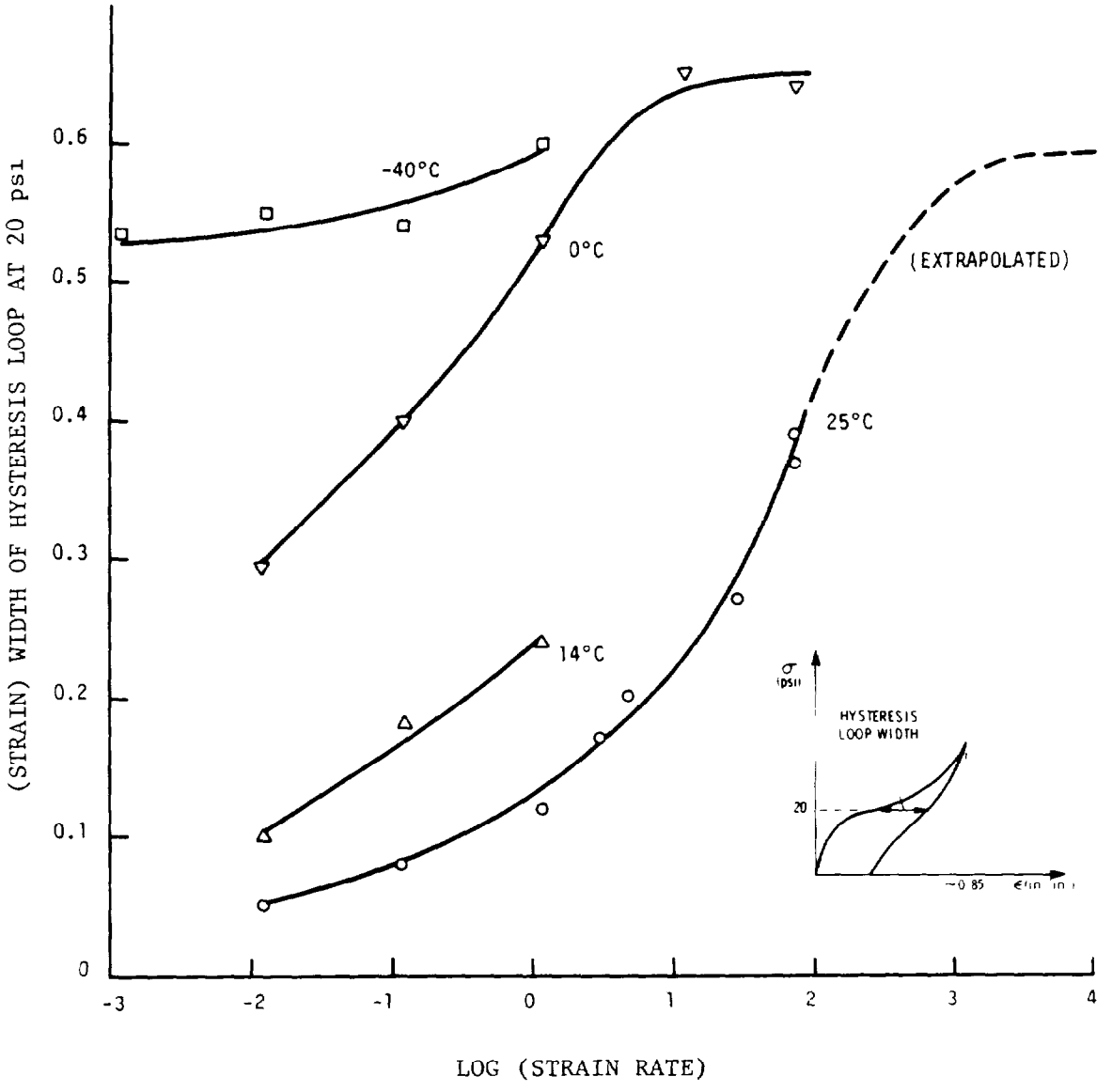

FIGURE 3-4. WIDTH OF HYSTERESIS LOOP AT 20 PSI

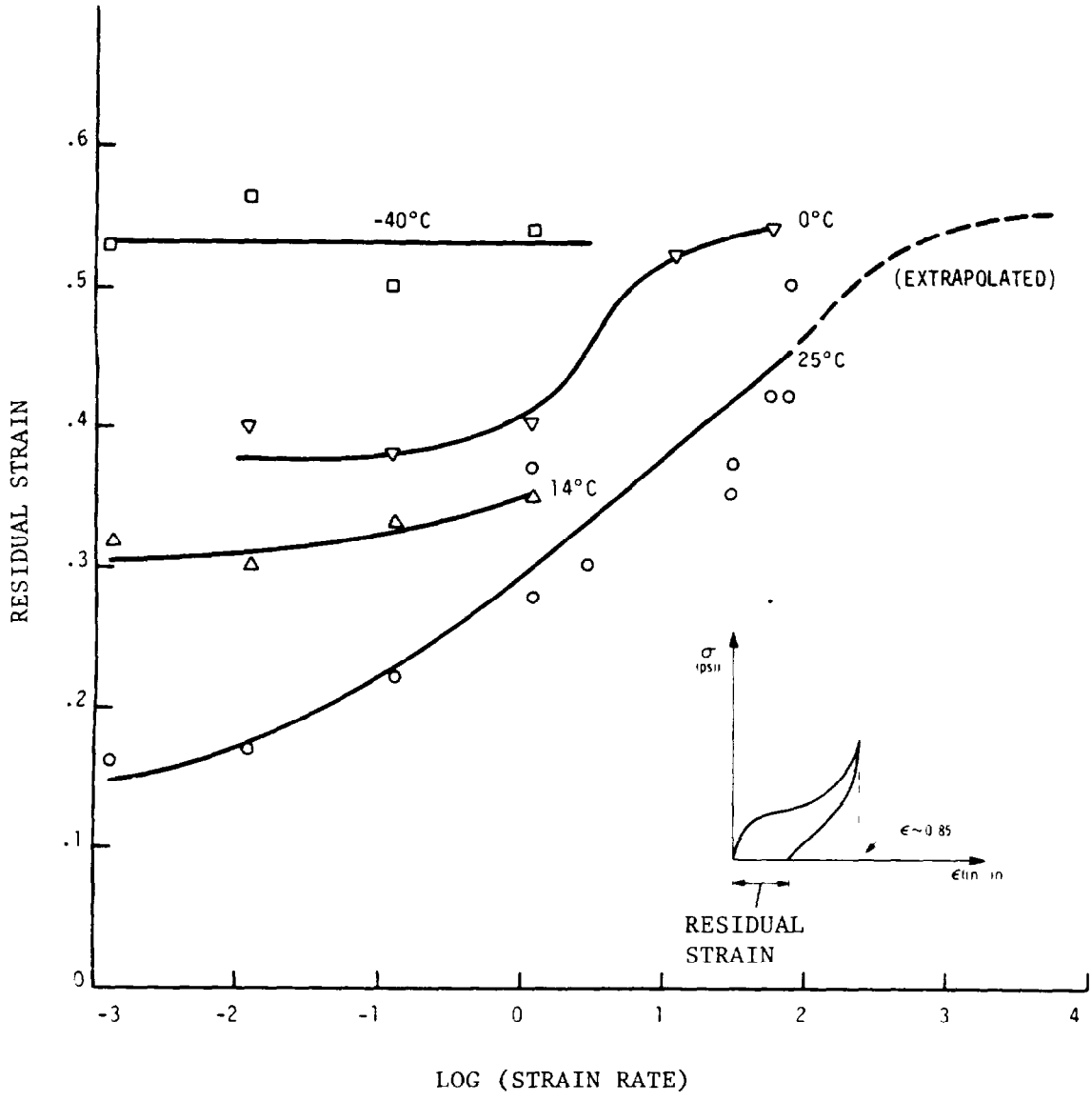

FIGURE 3-5. RESIDUAL STRAIN AFTER UNLOADING FROM 80-85% MAXIMUM STRAIN

correlate with the time, $\varepsilon / \dot{\varepsilon}$, to reach the same stress in a stress-strain test. A comparison can be made, therefore, by replotting the stress-strain master curves in terms of $\varepsilon/\dot{\varepsilon}$ instead of $\dot{\varepsilon}$.

Figure 3-6 compares the previously given master curves on this basis. Since the stress-strain specimen is at a strain close to the maximum for a very short part of the total test time to that point, as compared with a relaxation test where the entire test time is at the maximum strain, it is expected that the stress will be higher for relaxation at high strains. Consistent with this expectation, the stress-strain master curves in Figure 3-6 do fall above the relaxation master curves. Also as expected, the trends of both sets of curves are similar. In fact, the curves are sufficiently close that the simple expedient of shifting the stress-strain master curves half a decade to the left would allow prediction of the relaxation curves within the experimental uncertainty. This is a significant point, since only the stress-strain tests can be conducted at actual impact rates without the need for time-temperature shifting.

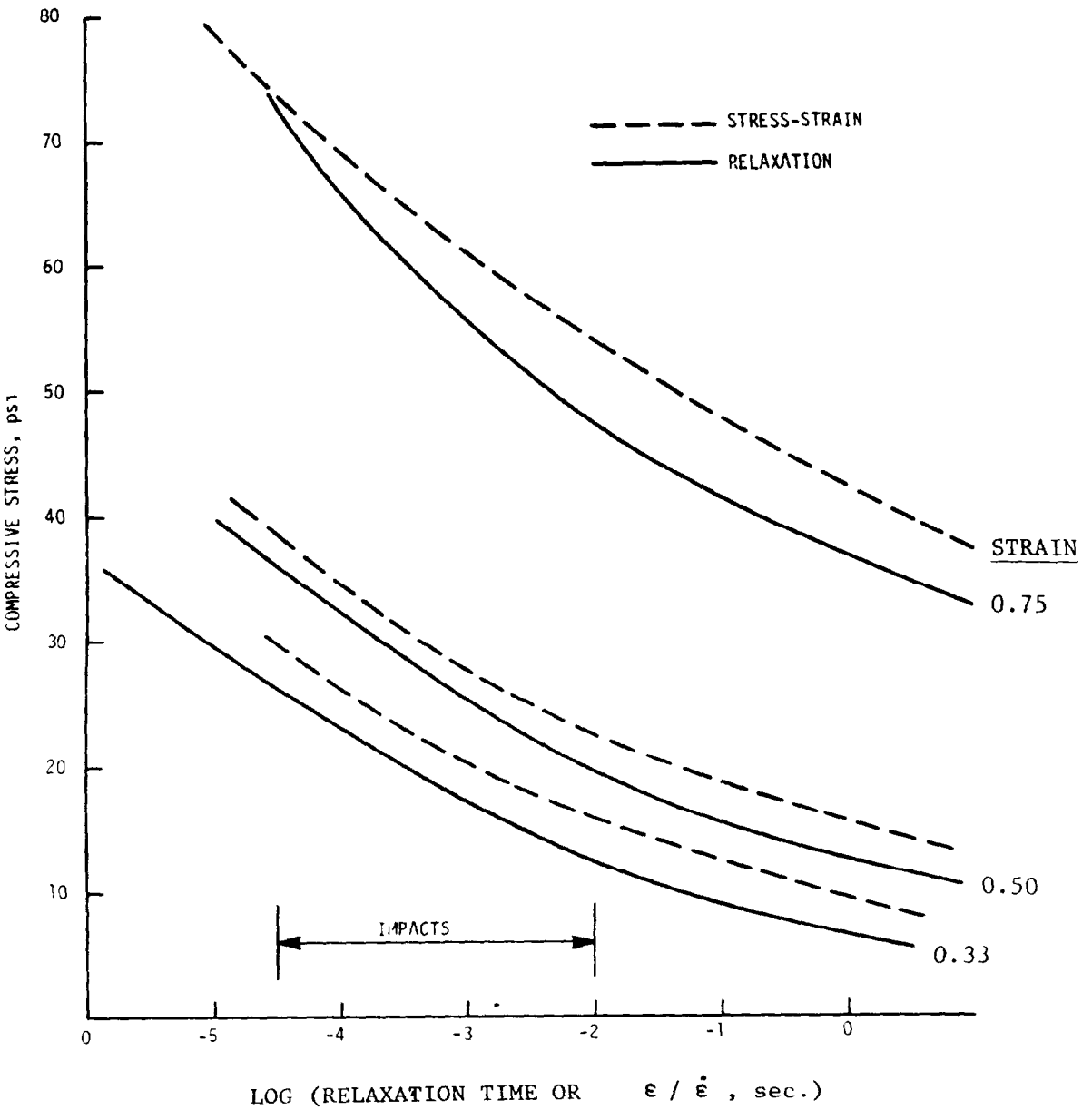

FIGURE 3-6. COMPARISON OF MASTER CURVES FROM STRESS-RELAXATION AND STRESS-STRAIN TESTS

4. OTHER EXPERIMENTS

The data discussed in Sections 2 and 3 provide the basis for a one-dimensional (uniform compression) constitutive equation model of Ensolite AAC. The validity of the model in one dimension depends upon the validity of an extrapolation procedure (time-temperature superposition) to infer material behavior at impact rates. One deviation of the data from the extrapolation was noted in Section 2.4 (see Figure 2-3). The utility of the model for collision analysis depends upon the influence of three-dimensional material characteristics under the nonuniform conditions involved in an occupant-to-vehicle impact. For these reasons, several additional experiments were performed on Ensolite AAC.

4.1 SPECIMEN DIAMETER EFFECTS

Even though Ensolite AAC is nominally a closed-cell foam, it is possible that air flow might contribute to the specimen stiffness under some conditions, and could significantly interfere with time-temperature shifting. Air flow effects, if present should be evident in tests of specimens with different diameters, since larger diameters would have longer air flow paths. The possibility of such an effect was investigated in a series of experiments where stress-strain curves were obtained for thin foam specimens of varying diameters, loaded at different strain rates.

Table 4-1 gives the stress during loading at three strain levels for various diameters and rates. The data do not appear to show any consistent trend with diameter; occasional higher stress at large diameters may be due to the increased constraint at the specimen/platen interface. Other parameters such as the permanent strain after unloading were similarly unaffected by diameter. These results suggest that air flow or any other diameter-dependent effects are not significant in Ensolite AAC, at least up to 0.75 strain.

TABLE 4-1. EFFECT OF SPECIMEN DIAMETER ON STRESS-STRAIN CURVE*

STRAIN RATE (SEC^{-1})	Dia (in.)	STRESS (psi)		
		Strain =0.3	Strain =0.5	Strain =0.75
73	2.0	18.5	30.2	85.1
	1.38	19.8	29.8	70.1
	1.0	19.7	29.9	68.5
30	3.9	21.1	30.2	63.9
	2.0	17.1	25.8	72.7
	1.38	16.1	26.2	71.9
	1.0	17.8	25.8	59.8
3.0	3.9	10.4	19.9	62.0
	2.0	10.4	18.2	50.9
	1.38	11.1	19.6	56.9
	1.0	11.4	19.6	54.9
	0.5	11.4	17.7	42.4
1.2	2.0	10.2	19.0	63.0
	1.38	10.6	19.5	70.3
	1.0	10.7	18.9	56.0

*Compression tests at 25°C; 0.14-inch thick specimen.

4.2 PERFORMANCE AT HIGH STRAIN AND LOW TEMPERATURE

The shifting anomaly observed for the long-time tails of stress-relaxation tests at 0.75 strain was studied further. After equilibrating at -20°C for 30 minutes, small rectangular thin-foam specimens were subjected to clamping at 0.75 or larger strain across half their length, with the other half left undeformed. Specimens were held clamped at -20°C for 20 to 30 minutes, released, and immediately sliced lengthwise with a razor to expose a cross-section containing both deformed and undeformed material. The surfaces of the deformed half appeared rough and pitted. Observation of the cross section under a low-power microscope revealed cell-wall crushing (Figure 4-1). The deformed cells were flattened and rough-edged compared to the round bubble shape of normal cells (Figure 4-2). The deformed half of the specimen remained collapsed for a long time. Even after two days strains of 0.15 to 0.25 were still evident. Within a week, however, the two halves were indistinguishable.

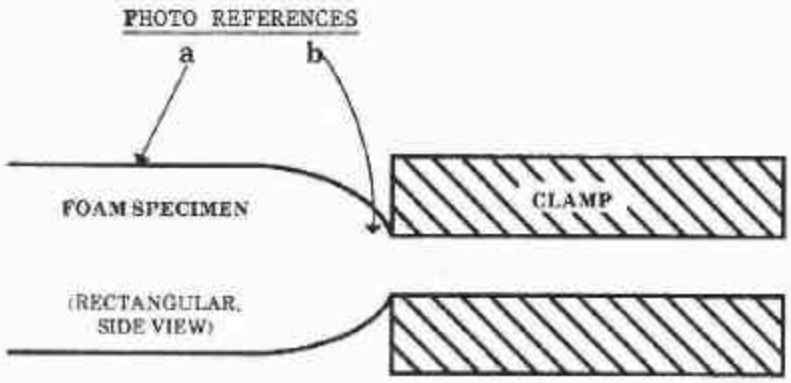

(A) SCHEMATIC OF CLAMPING TEST.

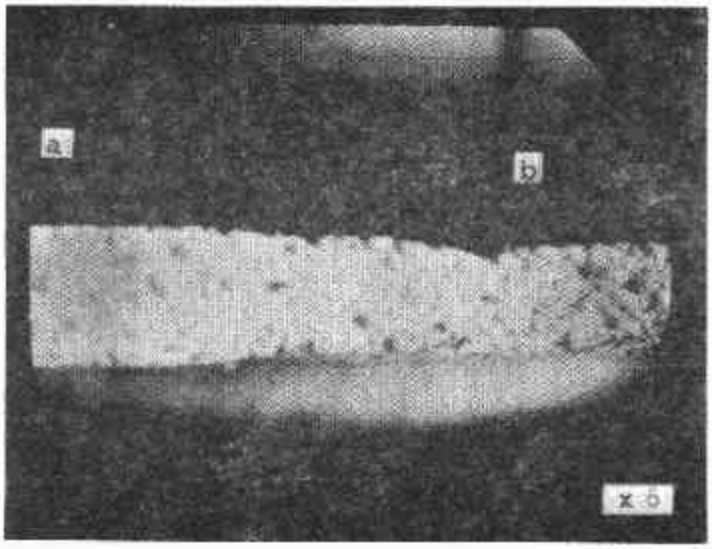

(B) APPEARANCE OF TEST SPECIMEN APPROXIMATELY 30 MINUTES AFTER REMOVAL FROM CLAMP AND COLD SOAK.

FIGURE 4-1. CLAMPING TEST CONFIGURATION AND RESULT

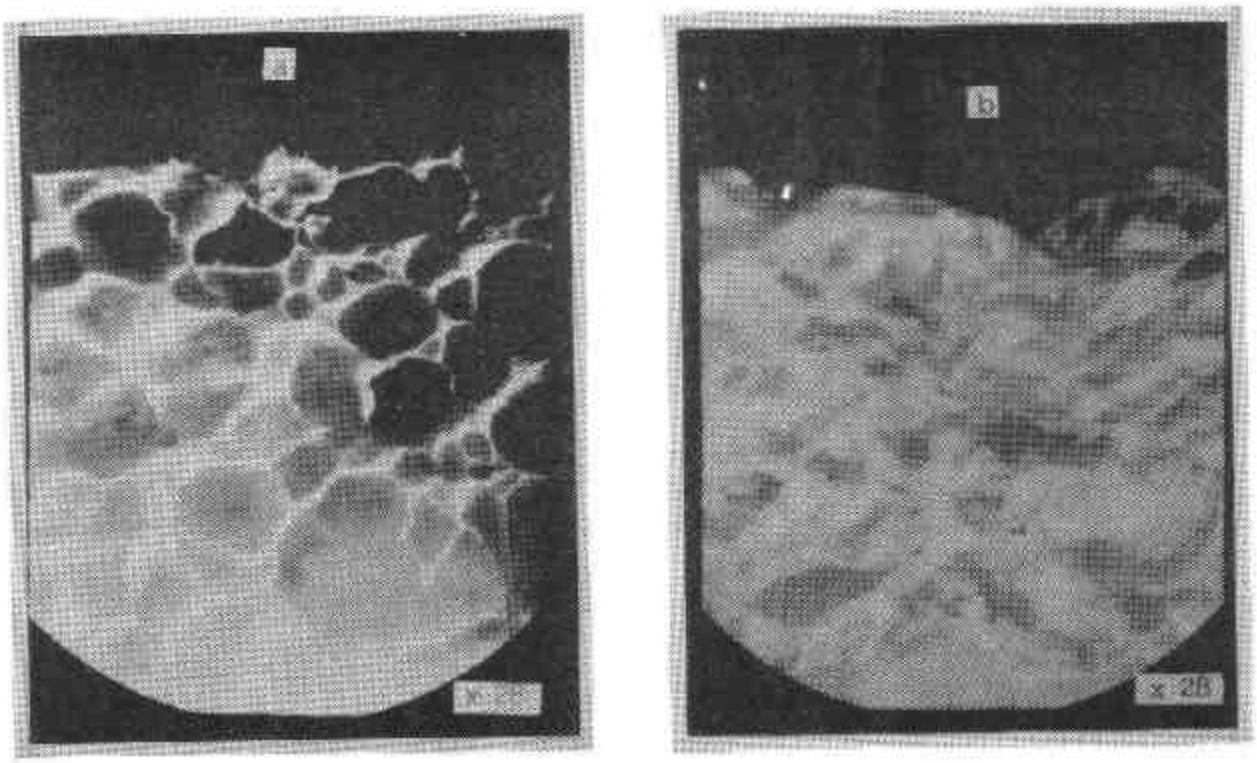

(A) NORMAL

(B) CRUSHED

FIGURE 4-2. COMPARISON OF NORMAL AND CRUSHED CELL WALLS

The cell-wall crushing phenomenon was observed only under combined conditions of high strain and low temperature, i.e. the same conditions under which the stress-relaxation test data deviated from the master curves. Neither of these phenomena is time-temperature shiftable, and the stress-relaxation deviations were consequently deemed to be inapplicable to impact-rate behavior at normal temperatures.

4.3 THICK FOAM BEHAVIOR

Ensolite AAC foam material of 1.2-inch thickness was tested for comparison with the thin material, and also to obtain directional properties of the foam. Unlike the thin material, the thick foam has a thin skin on the top and bottom surfaces. Specimens were approximately 1.2-inch cubes, with the xy-plane defined as parallel and the z-axis defined as perpendicular to the two skinned surfaces. The EM machine was used, with no special treatment to reduce friction at the platen interfaces. Figure 4-3 compares the stress-strain curves and shows the thick foam to be slightly stiffer parallel to the skin than in the z-direction. Also, the thick foam is generally on the order of 50 percent stiffer than the thin foam in the same range of strain rate.

Poisson's ratios were also measured by means of extensometry, since there was no a priori reason to assume that Ensolite foam would be an isotropic material. Table 4-2 summarizes these results.

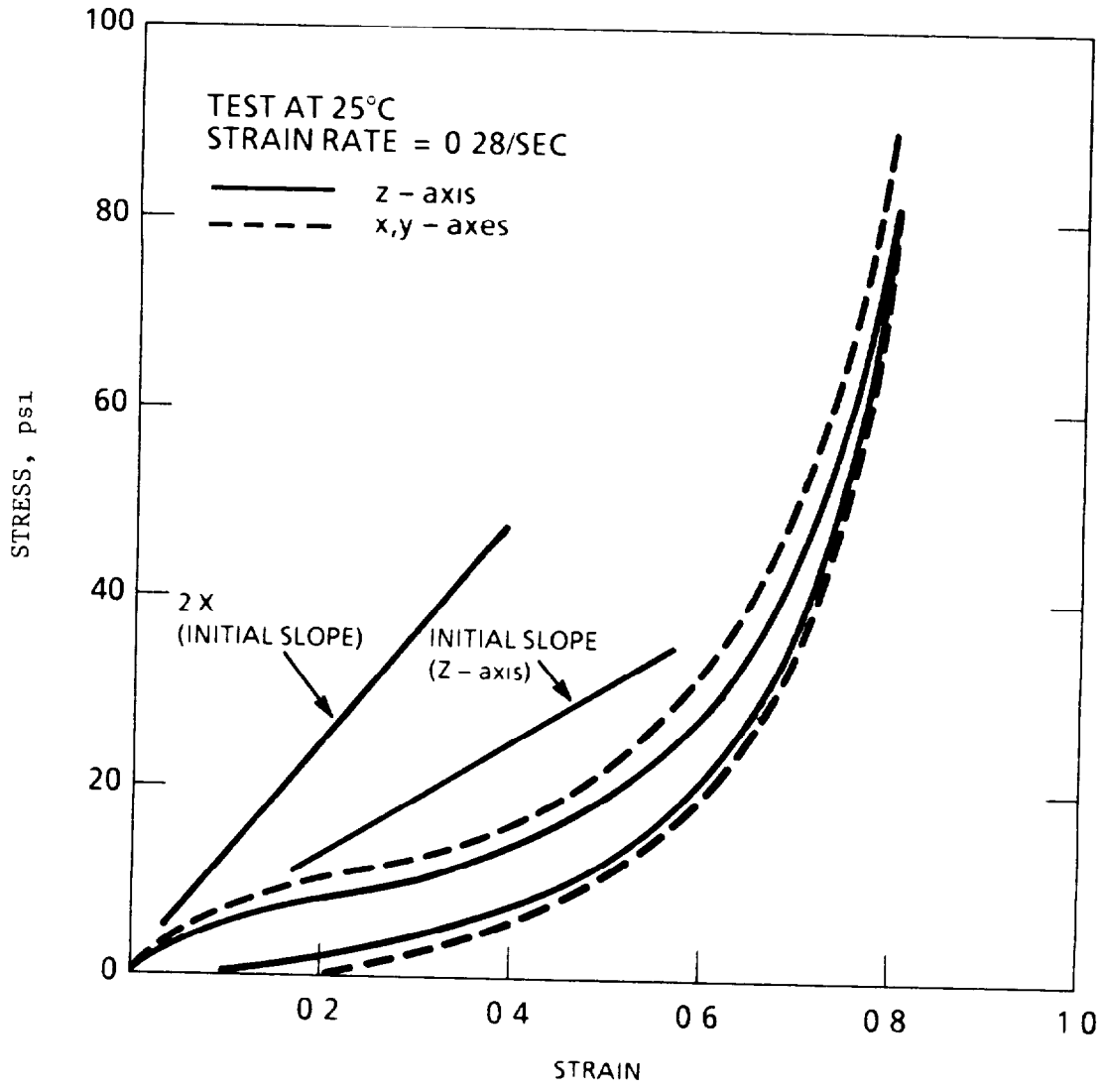

FIGURE 4-3. THICK FOAM STRESS-STRAIN CURVES

TABLE 4-2. POISSON'S RATIOS MEASURED ON BLOCKS OF THICK FOAM

Strain	υ_{xz}	υ_{yz}	υ_{xy}	υ_{yx}	υ_{zx}	υ_{zy}
0.5	0.326	0.352	0.122	0.138	0.152	0.168
0.5	0.312	0.300	0.138	0.159	0.132	0.170
0.5	0.258	0.400	0.168	0.150	0.142	0.120
0.5					0.162	0.150
0.2		0.47		0.120	0.185	0.185
0.4		0.43		0.100	0.140	0.200
0.6		0.40		0.150	0.130	0.184
0.8		0.48		0.150	0.170	0.220
Average	0.300	0.350	0.143	0.145	0.150	0.160
Standard Deviation	0.029	0.041	0.019	0.011	0.015	0.020

The idealized model of a linearly elastic and transversely isotropic material can be used to shed some light on the results of the thick-foam experiments. Transverse isotropy means that the elastic constants are isotropic in one plane but have different and independent values with respect to the axis normal to that plane. The processing o Ensolite foam in skinned sheets suggests that its physical symmetries should correspond to transverse isotropy with respect to the xy-plane and z-axis.

The elastic tension-compression stress-strain relations for a transversely isotropic material are given by [4] :

$$\varepsilon_x = (\sigma_x - \nu\sigma_y - \nu_z\sigma_z)/E \qquad (5)$$

$$\varepsilon_y = (\sigma_y - \nu\sigma_x - \nu_z\sigma_z)/E$$

$$\varepsilon_z = (\sigma_z - \nu_z^*\sigma_x - \nu_z^*\sigma_y)/E_z$$

where E, E_z, ν, and ν_z are independent constants, and where:

$$\nu_z^* = (l_z/l)\nu_z \tag{6}$$

In terms of the material measurements, E represents Young's modulus for in-plane loading, E_z represents Young's modulus for loading parallel to the z-axis and:

$$\begin{aligned} \nu &= \nu_{xy} = \nu_{yx} \\ \nu_z &= \nu_{xz} = \nu_{yz} \\ \nu_z^* &= \nu_{zx} = \nu_{zy} \end{aligned} \tag{7}$$

with respect to Table 4-2.

The average values for the Poisson's ratios in Table 4-2 are consistent with Equations 7, within experimental error. This observation, together with the fact that the Figure 4-3 stress-strain curves are identical for the x- and y-directions, strongly suggest that Ensolite foam is a transversely isotropic material.

The ratio of transverse to in-plane properties expressed by Equation 6, however, does not appear to be followed by Ensolite. The data in Table 4-2 suggest that ν_z is about 0.30 to 0.35, and that ν_z^* is about 0.15 to 0.16. thus, one would expect from Equation 6 that the ratio E/E_z should be about 2, i.e. that the in-plane stress-strain curve should exhibit about twice the stiffness of the z-axis curve in Figure 4-3.

Straight lines have been drawn on this figure to show the initial modulus of the z-axis curve and a slope twice as great. It is apparent that the initial modulus of the in-plane stress-strain curve fails to agree with the ratio relation, and the same can be said of any comparison of secant or tangent moduli at finite strains. Hence, there remains open a question of how the viscoelastic properties of Ensolite foam might be fully reconciled with the property of transverse isotropy.

4.4 GEOMETRY EFFECTS

The ability of a material to transfer load by means of shear is another three-dimensional property which may influence the material's response to impact. The stress-relaxation and stress-strain tests discussed in Sections 2 and 3 were free of shear, except for minor edge effects, since the platen diameters exceeded the specimen diameter.

The effect of shear was demonstrated by means of a series of stress-strain tests in which the load was applied through a flat-faced cylindrical indenter to specimens of the same diameter and to specimens with five times the indenter diameter. Table 4-3 summarizes the test details and the response forces which were measured at several combinations of strain and strain rate. The ratios of force in the large specimen to force in the small specimen are also plotted as "stiffness ratio at 5xD" in Figure 4-4.

The results show that there is only a small shear effect in the thin (0.14-inch thick) foam. The thick foam, however, exhibits an apparent stiffness of 1.8 to 2.7 times the uniform-compression stiffness over a straight-rate range of 0.5 to 2.2 per second. The increase in apparent stiffness is insensitive to strain rate in this range, but shows a strong tendency to decrease at high strain. These characteristics are typical of the stiffening effect produced by shear-transfer of loads.

Some additional stress-strain tests were performed at low strain rate to evaluate the relative stiffness contributions of shear and "bulk" behavior. "Bulk" stiffness refers to the material property under hydrostatic conditions ($\sigma_x = \sigma_y = \sigma_z$). For example, solid rubber materials typically have bulk moduli 10 to 100 times as large as their uniaxial compression moduli, and the bulk behavior increases the apparent stiffness when the material is subjected to lateral constraint.

A similar effect is possible in foam rubbers. The material per se provides some lateral constraint, for example, when subjected to the indenter test. The bulk behavior effect can be isolated by applying rigid constraints to a specimen subjected to uniform compression. Figure 4-5 compares the stress-strain curve for uniform

TABLE 4-3. INDENTER STRESS-STRAIN TEST DATA

CASE*	STRAIN	STRAIN RATE (sec^{-1})	FORCE (lb.)		RATIO LARGE/ STD
			STD**	LARGE DISK***	
Thick, no skin	0.25	2.2	10	27	2.57
Thick, skin	0.25	2.2	14	36	2.70
Thick, skin	0.25	0.55	8	20	2.50
Thin	0.25	0.48	5.7	8	1.40
Thick, no skin	0.50	2.2	22	58	2.63
Thick, skin	0.50	2.2	2.8	71	2.53
Thick, skin	0.50	0.55	21	47	2.24
Thin	0.50	0.48	13.7	18.2	1.33
Thick, no skin	0.75	2.2	61	121	1.98
Thick, skin	0.75	2.2	78	151	1.93
Thick, skin	0.75	0.55	63	116	1.84
Thin	0.75	0.48	40	49	1.24

*Thick: Ensolite AAC Foam, 1.2 in. thick (contains surface skin)
Thin: Ensolite AAC Foam, 0.14 in. thick.
Skin Removed: Skin removed with razor on surface to be loaded.
**Standard: 1.18 in. diameter specimen loaded in compression
***Large Disk: 5.9 in. diameter on flat support, loaded in center with 1.18 in. diameter flat end of rod.

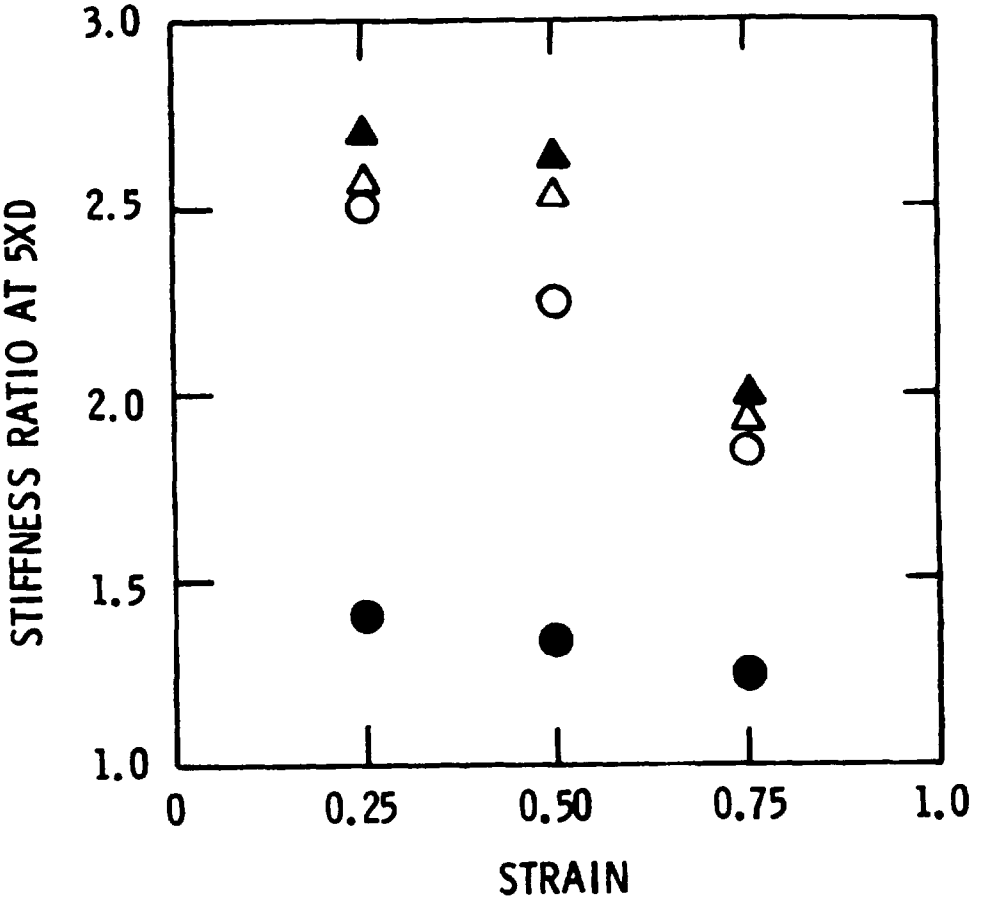

STRAIN RATE(SEC^{-1})	THICK		THIN
0.48	Without skin	With skin	●
0.55	○		
2.20	△	▲	

FIGURE 4-4. RESULTS OF INDENTER TESTS

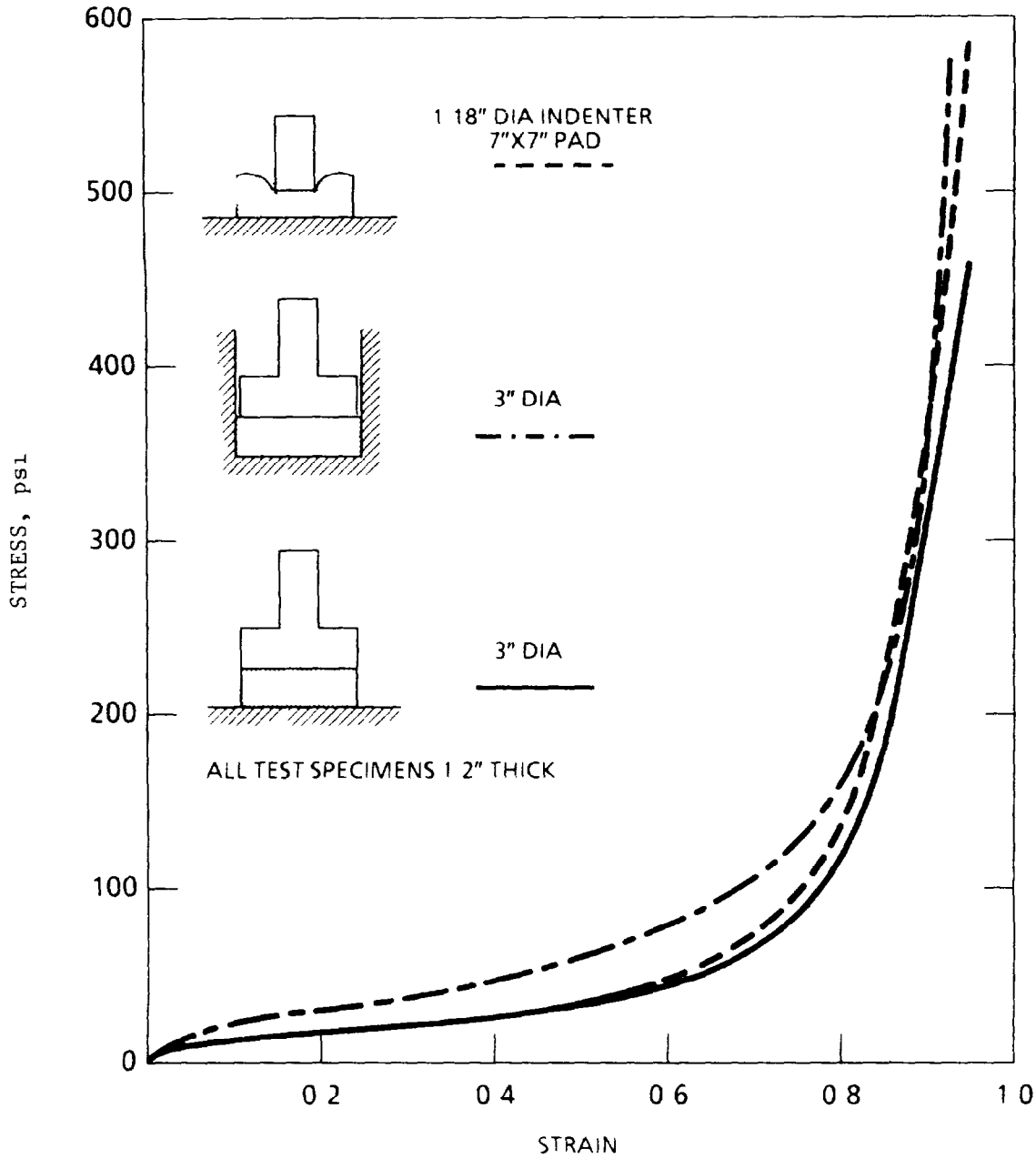

FIGURE 4-5. COMPARISON OF SHEAR AND BULK EFFECTS ON STIFFNESS

(unconstrained) compression with the curves for the indenter and bulk behavior tests. These data show that a true shear effect is dominant for strains up to about 0.8, but for larger strains, the bulk behavior dominates the increase of apparent stiffness.

The flat-edged indenter and bulk behavior tests overemphasize the effects of shear and constraint, relative to typical occupant-to-vehicle impacts, which are better represented by rounded indenters and partial constraint by surrounding material. Hence, in modelling a collision one should expect these three-dimensional effects to lie between the extremes and the idealization of uniform uniaxial compressive behavior.

A final question about three-dimensional effects concerns stress-relaxation behavior. If the material is assumed to possess distinct characteristic decay times for shear and bulk behavior, then the decay time measured in an experiment should depend of the test geometry.

In order to assess this question, stress-relaxation tests were performed at 0.75 strain with four different test geometries. In three of the tests, contiguous specimens of Ensolite foam were subjected to uniform compression, the flat-edged indenter, and a hemispherical indenter.

In the fourth test, the foam was pre-cut into 0.5-inch square columns, which were subjected as a group to the hemispherical indenter. The purpose of the fourth test was to simulate a popular modelling approach, in which it is assumed that contiguous material behaves as if it were a collection of independent columns subjected to different amounts of uniform compression [5] .

Figure 4-6 summarizes the results of these stress-relaxation tests. The data was left in terms of force rather than stress, and has been normalized for the purpose of comparison. For each test, the force-time history F(t) has been arbitrarily divided by F(10), the force measured at 10 seconds after strain application. Thus, all four test curves have been forced to pass through the normalizing point, and deviations between the curves at other times would indicate that the characteristic relaxation time depends on test geometry. It is apparent from the plot, however, that no such deviations occur.

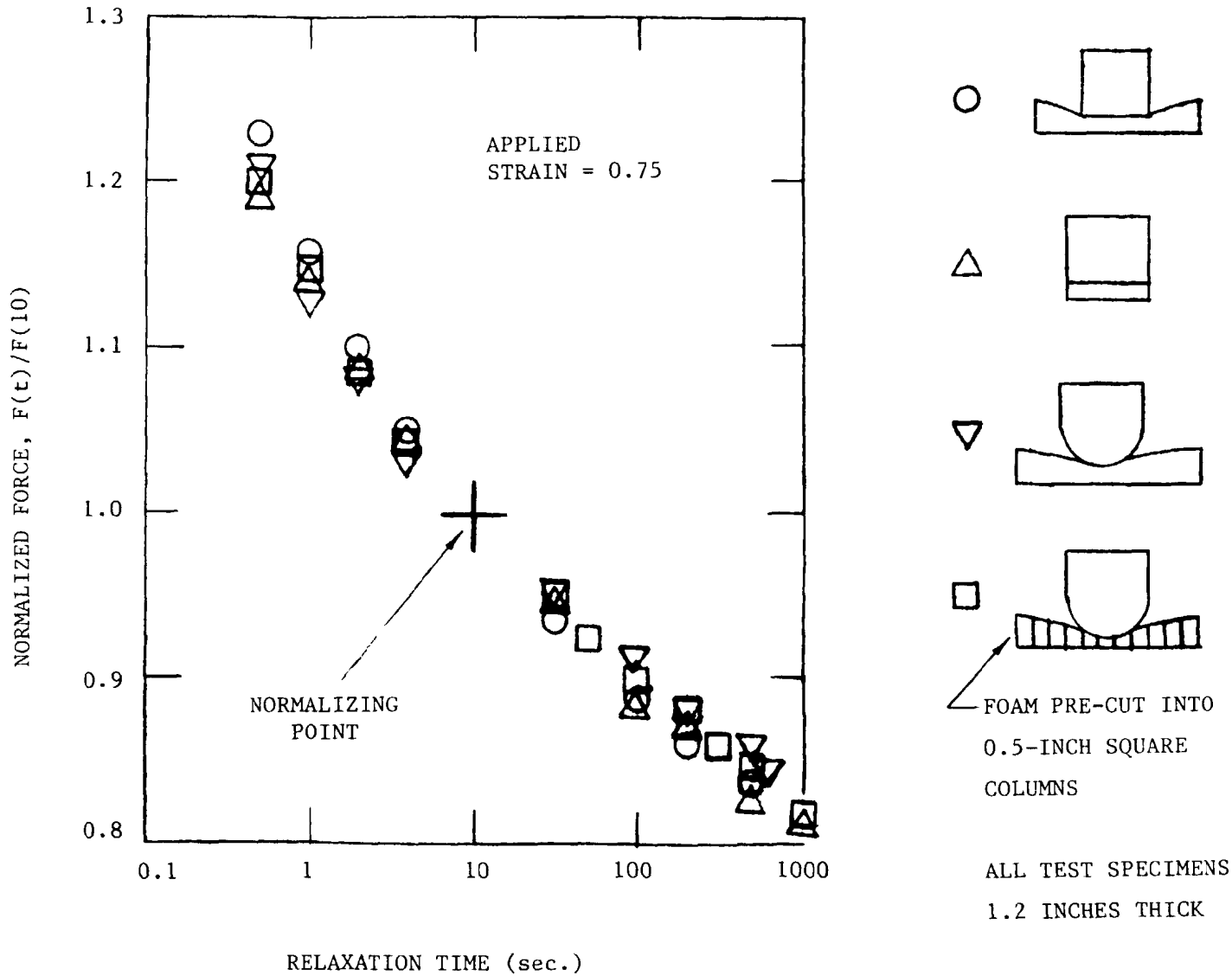

FIGURE 4-6. EFFECT OF INDENTER GEOMETRY ON RELAXATION CHARACTERISTIC

5. CONCLUSIONS

The research reported herein comprises an investigation of the dynamic properties of Uniroyal Ensolite AAC foam rubber. The research objective was to obtain the minimum data required as a basis for a constitutive equation model which could be used to predict the material response during typical occupant-to-vehicle impacts which may occur in automobile collisions.

Sufficient data has been gathered to provide the basis for one-dimensional (uniform uniaxial) dynamic compression models of Ensolite AAC. The required data has been tabulated in Appendices A and B. The following conclusions can be drawn from the results of the research:

- Ensolite AAC foam is a nonlinear viscoelastic material with dynamic characteristics which depend strongly on strain rate. The strain-rate effect also appears as a time effect, i.e. dynamic response at short times after a loading event is equivalent to dynamic response at high strain rates.

- Both stress-relaxation tests and stress-strain tests at constant strain rate are required to characterize the material in one dimension. The need for both types of test arises from the material nonlinearity.

- It is essential to assess stress-relaxation performance at short times (of the order of 0.1 to 10 milliseconds) and stress-strain curve performance at high strain rates (of the order of 2000 per second) to provide the basis for simulating typical impacts. These performance characteristics cannot be arbitrarily extrapolated from long-time or low-rate data. Some extrapolation is necessary, however, to cover impact rates which cannot be directly tested.

- The time-temperature superposition principle can be used to make the necessary extrapolations, if the principle is carefully applied. Careful application requires auxiliary tests to assess potential deviations.

- The dynamic properties of Ensolite foam are generally time-temperature shiftable, i.e. low-rate or long-time response at low temperature is equivalent to high-rate or short-time response at service temperature. Thus, it is possible to construct master curves for dynamic performance at service temperature. There are, however, two exceptions to this conclusion.

- The first exception involves stress-relaxation performance at times exceeding 100 seconds. At these very long times, Ensolite foam appears to have a decay characteristic different from the short-time characteristic. It is necessary, therefore, to focus on the short-time data in order to estimate asymptotic response parameters that will be useful in models of impact phenomena.

- The second exception involves performance at high strain (strain equal to or greater than 0.75). At these strain levels, Ensolite foam experiences a cell-wall crushing mode at low temperature, but the crushing mode is apparently absent under conditions of high strain rate at service temperature. Auxiliary tests were required to identify the crushing mode.

- Auxiliary tests were also required to show that the material does not possess any other non-shiftable characteristics, such as air-flow effects on stiffness. The presence or absence of such effects can be confirmed by varying the specimen diameter.

- Other auxiliary tests for Poisson's ratio and for different indenter geometries are useful for assessing some of the three-dimensional characteristics of foam-rubber materials.

- Ensolite foam appears to behave like a transversely isotropic material, but does not fully satisfy the static conditions of transverse isotropy. Further study of the viscoelastic effects on this property would be needed to provide the basis for a three-dimensional constitutive equation model.

- Under nonuniform one-dimensional loading, the apparent stiffness of Ensolite foam is increased by shear effects at strains up to 0.8 and by hydrostatic effects at strains exceeding 0.8. However, neither effect appears to influence the characteristic relaxation time.

- It appears that a one-dimensional constitutive equation for Ensolite foam, based on the uniform compression test results, will be useful for predicting occupant-to-vehicle impact responses.

- The sequence of basic and auxiliary tests reported herein form an experimental protocol which can be usefully applied to the characterization of other crash padding materials.

APPENDIX A
STRESS-RELAXATION TEST RESULTS

A.1 Basic Data

Tables A-1 through A-4 summarize the results of the stress-relaxation tests of Ensolite AAC. Table A-1 contains the 25°C shortest-time data, which extends from 5 ms to 0.4 second, and thus partly overlaps the impact range. Note that the time scale in this and the succeeding tables is given in $\log_{10}$ (time) values. Tables A-2 through A-4 contain data taken at several temperatures, and at times ranging from short (0.13 second) to long (316 seconds). Each of these tables covers one of the selected values of imposed strain (0.33, 0.50, and 0.75).

TABLE A-1. SHORT-TIME STRESS-RELAXATION DATA (25°C)

LOG(T) (sec)	STRAIN = 0.33		STRAIN = 0.50		STRAIN = 0.75	
	TEST A	TEST B	TEST A	TEST B	TEST A	TEST B
-2.3	12.5	16.6	20.0	22.8	48.5	50.0
-2.0	11.2	13.8	17.2	21.0	44.3	44.5
-1.7	9.0	10.2	14.4	16.0	41.4	38.3
-1.4	8.0	8.2	13.4	13.0	40.8	32.8
-1.1	7.4	7.6	12.6	12.1	37.9	37.2
-0.9	7.0	7.1	12.2	11.6	37.3	29.2
-0.8		7.0				
-0.77						29.0
-0.75				11.2		
-0.7	6.4		11.6		36.3	
-0.4	5.9		10.3		35.0	

TABLE A-2. LONG-TIME STRESS-RELAXATION DATA (STRAIN = 0.33)

log (t) (sec)	STRESS (psi)			
	-10°C	1°C	14°C	25°C
*	61.0	42.6	25.1	17.1
-0.9	33.1	17.2	10.3	8.7
-0.8	32.7	16.6	9.9	8.5
-0.7	32,1	16.0	9.6	8.0
-0.6	31.6	15.7	9.2	7.9
-0.5	31.0	15.0	8.7	7.8
-0.4	30.5	14.5	8.3	7.6
-0.3	29.6	13.9	8.1	7.3
-0.2	28.9	13.5	7.6	7.2
-0.1	28.2	13.1	7.4	7.0
0	27.5	12.8	7.2	6.9
0.1	26.9	12.2	6.9	6.7
0.2	26.2	11.7	6.8	6.6
0.3	25.5	11.3	6.5	6.4
0.4	24.8	11.0	6.2	6.2
0.5	24.1	10.6	6.1	6.2
0.6	23.5	10.1	5.8	6.0
0.7	22.7	9.8	5.6	5.7
0.8	22.0	9.6	5.6	5.6
0.9	21.5	9.4	5.5	5.5
1.0	20.9	8.8	5.3	5.4
1.1	20.3	8.6	5.3	5.3
1.2	19.6	8.2	4.7	5.2
1.3	19.1	7.9	5.1	5.1
1.4				5.1
1.5				4.9
1.54				5.0
1.75	16.3	7.2		
2.0	14.7	6.6		
2.5	12.2	5.5		

*First reading at approximately 14 ms.

TABLE A-3. LONG-TIME STRESS-RELAXATION DATA (STRAIN = 0.50)

log (t) (sec)	STRESS (psi)			
	-10°C	1°C	14°C	25°C
*	68.0	48.4	34.0	24.0
-0.9	37.1	22.4	18.2	13.7
-0.8	37.2	21.9	17.6	13.2
-0.7	35.9	21.3	17.2	13.6
-0.6	35.2	20.8	16.9	13.0
-0.5	34.6	20.2	16.5	12.8
-0.4	33.8	19.6	16.0	12.7
-0.3	33.6	18.9	15.7	12.7
-0.2	32.7	18.2	15.3	12.5
-0.1	31.9	17.8	14.9	12.1
0	31.3	17.3	14.7	11.9
0.1	30.6	16.6	14.4	11.8
0.2	30.0	16.3	14.0	11.4
0.3	29.2	15.7	13.7	11.1
0.4	28.4	15.3	13.3	11.1
0.5	27.6	14.8	13.2	11.0
0.6	27.0	14.5	12.9	10.9
0.7	26.3	14.5	12.6	10.8
0.8	25.8	14.0	12.2	10.8
0.9	25.2	13.6	12.1	10.6
1.0	24.5	13.1		10.4
1.1	24.0	12.8		10.3
1.2	23.2	12.5		10.1
1.3	22.8	12.1		9.9
1.5			11.0	9.8
1.6				9.7
1.65			10.9	9.5
1.75	19.7	10.7		
2.0	18.3	10.0	10.2	
2.5	15.1	8.6		
2.7			9.4	

*First reading at approximately 18 ms.

TABLE A-4. LONG-TIME STRESS-RELAXATION DATA (STRAIN = 0.75)

log (t) (sec)	STRESS (psi)			
	-10°C	1°C	14°C	25°C
*	130.0	73.5	83.4	64.6
-0.9	80.8	35.8	50.6	41.2
-0.8	71.8	34.8	49.8	40.4
-0.7	70.4	34.4	49.1	39.5
-0.6	68.4	33.7	48.5	39.4
-0.5	67.0	33.2	47.7	38.2
-0.4	66.2	32.7	47.0	38.0
-0.3	65.2	31.9	46.6	37.6
-0.2	63.9	31.3	46.1	37.7
-0.1	62.7	30.8	45.6	36.3
0	62.4	30.2	45.0	35.9
0.1	61.0	29.6	44.4	35.7
0.2	59.5	28.9	43.9	35.7
0.3	58.1	28.4	43.1	35.2
0.4	56.9	28.0	42.7	34.8
0.5	55.8	27.4	42.1	34.6
0.6	55.1	26.7	41.4	34.4
0.7	53.6	25.9	41.0	34.0
0.8	52.2	25.1	40.4	33.6
0.9	51.0	24.8	40.1	33.1
1.0	49.7	24.4	39.6	32.4
1.1	48.4	23.5	39.0	31.7
1.2	47.4	23.1	38.6	31.3
1.3	45.8	22.8	38.3	30.7
1.4				31.0
1.5				30.6
1.6				30.4
1.75	40.4	20.9	36.2	
2.0		19.7		
2.5	29.5	17.6	33.2	

*First reading at approximately 25 ms.

Asymptotic Data

It is possible in principle to infer the asymptotic (zero strain-rate) stress-strain curve from a stress-relaxation test by taking data at sufficiently long times after the strain has been imposed. In practive, however, a material usually exhibits multiple relaxation mechanisms with different characteristic times, and asymptotes must be estimated with their ultimate use in mind. In the present case, the objective is a material model for the impact regime, but the Ensolite data exhibits at least one lone-time relaxation mechanism. Therefore, asymptotic parameters were estimated from the short-time data to intentionally focus the model basis on the impact regime. Table A-5 summarizes the asymptote estimates.

TABLE A-5. ESTIMATED STRESS-RELAXATION ASYMPTOTES

STRAIN	STRESS ASYMPTOTE(psi)			
	-10°C	1°C	14°C	25°C
.33	4.5	4.5	4.5	4.5
.50	7.0	7.0	7.0	8.5
.75	26.0	26.0	26.0	26.0

APPENDIX B

STRESS-STRAIN TEST RESULTS

Tabular Data

Tables B-1 through B-5 summarize the results of the low-rate EM stress-strain tests. The strain rate in Table B-1 is 5 to 6 orders of magnitude lower than impact rates. Hence, the data in this table can be considered a good approximation of the asymptotic (zero strain rate) material behavior. Table B-5 summarizes the results of the high-rate SH tests. Residual strains have been abstracted from Tables B-1 through B-5 and are presented in Table B-6.

TABLE B-1. ELECTROMECHANICAL STRESS-STRAIN DATA
(STRAIN RATE = 0.0012/sec)

STRAIN	STRESS (psi)							
	-40°C		0°C		14°C		25°C	
	LOAD	UNLOAD	LOAD	UNLOAD	LOAD	UNLOAD	LOAD	UNLOAD
.05	6		3		2		1	
.10	18		6		3		2	
.15	36		9		4		3	
.20	50		10		5		4	0
.25	55		11		6		4	1
.30	58		12		7	0	5	1.5
.35	60		14		8	1	6	2
.40	62		16		9	2	7	3
.45	65		19		11	4	8	5
.50	68		22		14	6	10	6
.52		0						
.55	72	2	27		17	9	13	9
.60	76	10	32		21	12	16	12
.65	81	23	39		27	16	20	16
.70	86	40	48		35	24	25	22
.75	94	65	61		46	35	30	28
.78							33	33
.79	100	100	77					
.80					62	55		
.81					67	67		

*No data taken.

TABLE B-2. ELECTROMECHANICAL STRESS-STRAIN DATA
(STRAIN RATE = 0.012/sec)

STRAIN	STRESS (psi)							
	-40°C		0°C		14°C		25°C	
	LOAD	UNLOAD	LOAD	UNLOAD	LOAD	UNLOAD	LOAD	UNLOAD
0.05	3		3		3		1	
0.10	13		10		5		2	
0.15	30		13		6		3	
0.16								0
0.20	45		14		7		4	0.5
0.25	56		15		8		5	1
0.30	61		16		9	0	6	1.5
0.35	62		18		10	2	7	2
0.40	63		20	0	12	4	8	4
0.45	65		22	2	14	6	9	5
0.50	68		26	4	17	8	11	7
0.55	71		30	6	20	10	14	9
0.56		0						
0.60	75	5	35	10	25	14	17	12
0.65	80	15	42	15	31	20	21	16
0.70	85	29	52	22	40	29	26	21
0.75	91	48	67	31	53	41	31	27
0.80	99	73	92	50	74	79	38	38
0.81					81	81		
0.84	106	106						
0.85			137	137				

TABLE B-3. ELECTROMECHANICAL STRESS-STRAIN DATA
(STRAIN RATE = 0.12/sec)

STRAIN	STRESS (psi)							
	-40°C		0°C		14°C		25°C	
	LOAD	UNLOAD	LOAD	UNLOAD	LOAD	UNLOAD	LOAD	UNLOAD
0.05	6		4		4		2	
0.10	19		13		7		3	
0.15	39		16		9		4	
0.20	55		18		10		5	0
0.25	63		19		11		6	1
0.30	65		21		12		7	1.5
0.32						0		
0.35	67		23		14	1	8	2.5
0.38				0				
0.40	70		25	1	16	2	9	4
0.45	72		29	3	18	4	11	5
0.50	76	0	32	5	21	6	13	7
0.55	79	5	37	9	25	10	16	9
0.60	83	12	43	12	30	13	19	12
0.65	87	23	53	17	36	19	21	17
0.70	93	42	64	26	45	27	25	21
0.75	100	67	83	40	59	40	32	28
0.80	112	112			80	60	40	38
0.81			122	122			41	41
0.83					97	97		

TABLE B-4. ELECTROMECHANICAL STRESS-STRAIN DATA
(STRAIN RATE = 1.12/sec)

STRAIN	STRESS (psi)							
	-40°C		0°C		14°C		25°C	
	LOAD	UNLOAD	LOAD	UNLOAD	LOAD	UNLOAD	LOAD	UNLOAD
0.05	12		9		2		2	
0.10	24		17		8		4	
0.15	38		23		10		6	
0.20	54		25		12		7	
0.25	65		27		14		8	
0.30	71		28		15		10	
0.35	76		30	0	17		11	
0.38								0
0.40	78		32	2	19	0	12	2
0.45	81		35	3	22	3	14	4
0.50	84		39	5	25	5	16	6
0.55	87	0	44	7	28	7	18	8
0.60	90	5	50	9	32	9	21	10
0.65	96	10	58	14	38	16	25	12
0.70	100	32	69	22	47	30	28	19
0.75	105	60	86	38	60	55	33	29
0.80	112	88	109	65	88	88	38	38
0.83			135	135				
0.85					109	109	44	44
0.86	121	121					46	46

TABLE B-5. SERVOHYDRAULIC STRESS-STRAIN DATA (25°C)

STRAIN	STRESS (psi)									
	1.2/sec		3.0/sec		7.5/sec		30/sec		73/sec	
	LD	UL	LD	UL	LD	UL	LD	UL	LD	UL
0.050	3		4		5		5		5	
0.010	6		7		9		10		13	
0.150	7		8		10		11		15	
0.200	9		9		11		13		15	
0.250	9		10		12		14		17	
0.275		0								
0.300	11	1	11	0	13	0	16		18	
0.350	12	2	13	2	15	1	18	0	20	
0.400	14	3	14	3	16	3	20	2	22	0
0.450	16	6	17	4	19	4	22	3	25	2
0.500	19	8	20	7	22	6	26	5	28	4
0.550	24	11	24	9	25	9	30	8	33	6
0.600	29	15	28	13	30	12	36	11	39	9
0.625	33		31		32		40		42	
0.650	37	22	34	18	36	17	44	16	46	13
0.675	43		39		39		49		51	
0.700	50	31	43	25	44	22	55	23	57	19
0.750	70	46	57	34	55	30	72	34	72	26
0.775	88	58	66	40	62	35	83	42	82	32
0.800	108	77	78	49	72	41	97	53	96	39
0.825	140	111	95	61	83	49	112	70	112	48
0.830	143	143								
0.833							115	115		
0.850			119	77	100	60			133	62
0.875			151	108	122	76			154	83
0.887									158	158
0.885			159	159						
0.900					148	109				
0.906					149	149				

TABLE B-6. RESIDUAL STRAINS AT ZERO STRESS

STRAIN RATE (sec^{-1})	T (°C)	-40	0	14	25
0.0012		0.52	-----	0.30	0.20
0.012		0.56	0.40	0.30	0.16
0.12		0.50	0.38	0.32	0.20
1.2		0.55	0.35	0.40	0.38 0.275*
3.0					0.30*
7.5					0.30*
30.0					0.35*
73.0					0.40*

*Servohydraulic data.

Shift Factors

Time-temperature shift factors were graphically derived from plots like Figures 2-2 and 3-2. The graphical procedure leads to different sets of empirical shift factors for stress-relaxation and stress-strain data. Figure B-1 summarizes the shift factors for both types of data.

REFERENCES

1) W. Flugge, Viscoelasticity, Blaisdell Publishing Company, Waltham, MA 1967

2) A. V. Tobolsky, Properties and Structure of Polymers, Wiley, New York, 1967.

3) I. M. Ward, Mechanical Properties of Solid Polymers, Wiley-Interscience, London, 1971.

4) W. F. Chen and A. F. Saleeb, Constitutive Equations for Engineering Materials, Volume 1: Elasticity and Modelling, Wiley-Interscience, New York, 1982.

5) F. J. Lockett, R. R. Cousins, and D. Dawson, "Engineering Basis for Selection and Crash Padding Materials," Plastics and Rubber Processing and Applications, Vol. 1 No. 1 (1981), 25-37.